World Journal of Gastroenterology

Submit a Manuscript: https://www.f6publishing.com

World J Gastroenterol 2024 August 7; 30(29): 3488-3510

DOI: 10.3748/wjg.v30.i29.3488

ISSN 1007-9327 (print) ISSN 2219-2840 (online)

ORIGINAL ARTICLE

Basic Study

Leech *Poecilobdella manillensis* protein extract ameliorated hyperuricemia by restoring gut microbiota dysregulation and affecting serum metabolites

Xia Liu, Xing-Qiu Liang, Tian-Cai Lu, Zhe Feng, Min Zhang, Nan-Qing Liao, Feng-Lian Zhang, Bo Wang, Li-Sheng Wang

Specialty type: Gastroenterology and hepatology

Provenance and peer review: Unsolicited article; Externally peer reviewed.

Peer-review model: Single blind

Peer-review report's classification

Scientific Quality: Grade A, Grade C

Novelty: Grade A, Grade B

Creativity or Innovation: Grade A, Grade B

Scientific Significance: Grade A, Grade C

P-Reviewer: Muntané J; Wang X

Received: March 10, 2024

Revised: June 20, 2024

Accepted: July 19, 2024

Published online: August 7, 2024

Processing time: 140 Days and 11.8 Hours

Xia Liu, Nan-Qing Liao, Feng-Lian Zhang, Bo Wang, Li-Sheng Wang, Medical College, Guangxi University, Nanning 530004, Guangxi Zhuang Autonomous Region, China

Xia Liu, Department of Traditional Chinese Medicine, HIV/AIDS Clinical Treatment Center of Guangxi (Nanning), The Fourth People's Hospital of Nanning, Nanning 530023, Guangxi Zhuang Autonomous Region, China

Xing-Qiu Liang, Department of Science and Technology, Ruikang Hospital Affiliated to Guangxi University of Chinese Medicine, Nanning 530011, Guangxi Zhuang Autonomous Region, China

Tian-Cai Lu, General Manager's Office, Guangxi Fuxinyi Biological Technology Co. Ltd., Pingnan 537300, Guangxi Zhuang Autonomous Region, China

Zhe Feng, Department of Joint and Sports Medicine, Ruikang Hospital Affiliated to Guangxi University of Chinese Medicine, Nanning 530011, Guangxi Zhuang Autonomous Region, China

Min Zhang, Department of Gerontology, Nanning Social Welfare Hospital, Nanning 530004, Guangxi Zhuang Autonomous Region, China

Corresponding author: Li-Sheng Wang, MD, PhD, Professor, Medical College, Guangxi University, No. 100 Daxue East Road, Nanning 530004, Guangxi Zhuang Autonomous Region, China. lswang@gxu.edu.cn

Abstract

BACKGROUND

Hyperuricemia (HUA) is a public health concern that needs to be solved urgently. The lyophilized powder of *Poecilobdella manillensis* has been shown to significantly alleviate HUA; however, its underlying metabolic regulation remains unclear.

AIM

To explore the underlying mechanisms of *Poecilobdella manillensis* in HUA based on modulation of the gut microbiota and host metabolism.

METHODS
A mouse model of rapid HUA was established using a high-purine diet and potassium oxonate injections. The mice received oral drugs or saline. Additionally, 16S rRNA sequencing and ultra-high performance liquid chromatography with quadrupole time-of-flight mass spectrometry-based untargeted metabolomics were performed to identify changes in the microbiome and host metabolome, respectively. The levels of uric acid transporters and epithelial tight junction proteins in the renal and intestinal tissues were analyzed using an enzyme-linked immunosorbent assay.

RESULTS
The protein extract of *Poecilobdella manillensis* lyophilized powder (49 mg/kg) showed an enhanced anti-trioxypurine ability than that of allopurinol (5 mg/kg) ($P < 0.05$). A total of nine bacterial genera were identified to be closely related to the anti-trioxypurine activity of *Poecilobdella manillensis* powder, which included the genera of *Prevotella*, *Delftia*, *Dialister*, *Akkermansia*, *Lactococcus*, *Escherichia_Shigella*, *Enterococcus*, and *Bacteroides*. Furthermore, 22 metabolites in the serum were found to be closely related to the anti-trioxypurine activity of *Poecilobdella manillensis* powder, which correlated to the Kyoto Encyclopedia of Genes and Genomes pathways of cysteine and methionine metabolism, sphingolipid metabolism, galactose metabolism, and phenylalanine, tyrosine, and tryptophan biosynthesis. Correlation analysis found that changes in the gut microbiota were significantly related to these metabolites.

CONCLUSION
The proteins in *Poecilobdella manillensis* powder were effective for HUA. Mechanistically, they are associated with improvements in gut microbiota dysbiosis and the regulation of sphingolipid and galactose metabolism.

Key Words: Gut microbiota; Metabolism; Multi-omics; *Poecilobdella manillensis*; Sphingolipid metabolism pathway; Galactose metabolism pathway; Hyperuricemia

Core Tip: This study reveals the novel therapeutic potential of *Poecilobdella manillensis* in treating hyperuricemia (HUA) through a dual mechanism: The direct modulation of uric acid levels and restoration of renal and intestinal barriers. Importantly, it highlights the role of proteins in *Poecilobdella manillensis* in rectifying gut microbiota dysbiosis and adjusting key metabolic pathways, most notably, sphingolipid and galactose metabolism. These findings highlight the multi-target, multi-channel effects of *Poecilobdella manillensis* treatment for HUA and provide fundamental data for the clinical use of HUA treatments.

Citation: Liu X, Liang XQ, Lu TC, Feng Z, Zhang M, Liao NQ, Zhang FL, Wang B, Wang LS. Leech *Poecilobdella manillensis* protein extract ameliorated hyperuricemia by restoring gut microbiota dysregulation and affecting serum metabolites. *World J Gastroenterol* 2024; 30(29): 3488-3510
URL: https://www.wjgnet.com/1007-9327/full/v30/i29/3488.htm
DOI: https://dx.doi.org/10.3748/wjg.v30.i29.3488

INTRODUCTION

Hyperuricemia (HUA) is a metabolic disorder characterized by abnormally elevated levels of uric acid (UA) in the bloodstream. HUA, often caused by purine metabolism disorders and UA metabolism disorders, tends to induce gout, and may also affect the urinary system[1]. A report detailing the trends in HUA and gout within China indicated that approximately 13.3% of the population is impacted by HUA, equating to around 177 million individuals[2]. Globally, the increasing incidence of HUA has resulted in it becoming one of the most common basal metabolic diseases[3]. Furthermore, accumulating evidence has shown that HUA plays a pivotal role not only in the development of gout, but also in diabetes mellitus, cardiovascular disease, hypertension, and chronic kidney disease[3]. Some studies have shown that HUA and gout are risk predictors of all-cause mortality from cardiovascular disease[4]. Given the harmful effects of HUA, there is an urgent need for a scientific understanding of the HUA pathogenesis and the identification of new therapeutic drugs.

The gut microbiota is crucial for the metabolism of HUA. Changes or imbalances in the composition of gut microbiota can lead to metabolic disorders throughout the body[5]. Approximately 70% of UA is eliminated *via* the kidneys, while the rest is primarily excreted in the feces or is further broken down by the gut microbiota[6]. A high-purine diet may influence the physiological state of the host through interactions with the gut microbiota[7]. Host metabolic function has been shown to be affected by changes in the structure and composition of the gut microbiota[8]. Exploring the pathogenesis of HUA using the gut microbiota as an entry point has become a new research hotspot worldwide. Early studies

have confirmed the relationship between the gut microbiota and metabolic changes in HUA[9-11], suggesting that changes in serum metabolism caused by the gut microbiota is a suitable strategy for HUA research.

Currently, medications for treating HUA comprise xanthine oxidase (XOD) inhibitors [such as allopurinol (AP) and febuxostat], recombinant urate oxidase (rasburicase), and promoters of UA excretion (benzbromarone)[12,13]. Although these drugs exhibit clinical efficacy, their side effects frequently restrict their usage in clinical settings. For instance, AP can provoke a deadly hypersensitivity syndrome[14], benzbromarone may cause hepatotoxicity[13], and rasburicase is known to trigger rapid hypersensitivity reactions[15,16]. Therefore, it is necessary to find valid, promising, and economical therapies for the treatment of HUA. Leeches (Hirudo) are part of traditional Chinese medicine, first seen in the "Shennong Materia Medica", a pharmacological treatise published in the Eastern Han Dynasty[17]. *Poecilobdella manillensis*, commonly known as the Philippine cattle leech or medical vermiculite in Manila, belongs to the genus of medicinal vermiculite leeches[18]. This larger species of leech is widely distributed throughout Southeast Asia, including regions in China, such as Guangxi. In China, medicinal vermiculite leeches that feed on animal blood include *Poecilobdella manillensis* and *Hirudonipponia whitma*[19]. Some studies have reported that their pharmacological effects include analgesic, anti-inflammatory, platelet-inhibitory, anticoagulant, and thrombin-regulatory functions, in addition to degradative effects on the extracellular matrix[18,20,21]. Limited studies have been performed to explore the efficacy of *Poecilobdella manillensis* on HUA and gout. Dong *et al*[22] reported that *Poecilobdella manillensis* lyophilized powder significantly reduced UA levels in HUA mice, whilst also proving to be safe for use. However, the active anti-HUA components, the *in vivo* metabolic mechanisms, and the molecular mechanisms of this treatment are not fully understood. In recent years, further research on leeches has identified the main components of leeches, which include proteins, polypeptides, some small molecular compounds, and trace elements[23]. Most studies have focused on the effect of single isolated polypeptides, such as hirudin[24,25], but not a mixture of different proteins, such as the leech total protein (LTP). Therefore, the mechanism by which LTP lowers UA has not yet been clarified, and no studies on the treatment of HUA with LTP currently exist.

To the best of our knowledge, there are no metabolomics and microbiome studies on the effects of LTP in HUA animals. Here, we aimed to reveal host serum metabolic changes, in addition to gut microbial changes, in the cecal contents of HUA mice. Furthermore, we aimed to reveal to possible mechanism through a combination of gut microbiota and metabolomics analyses.

MATERIALS AND METHODS

Chemicals and reagents

Experimental leech *Poecilobdella manillensis* freeze-dried powder (Place of origin: Pingnan of Guangxi, China) was supplied by Guangxi Fuxinyi Biological Technology Co., Ltd. (Pingnan, China). Potassium oxonate (PO) (purity ≥ 98.0%, P137112) and AP (purity ≥ 98.0%) were purchased from Shanghai Aladdin Biochemical Technology Co., Ltd. (Shanghai, China). The high-purine diet consisted of mice feedstuff (100 g), yeast extract (40 g), and yeast ribonucleic acid (2 g), which were re-granulated after melting the above ingredients, supplied by Jiangsu Xietong Pharmaceutical Bio-engineering Co., Ltd. (Nanjing, China). UA (C012-2-1), XOD (A002-1-1), creatinine (CRE, C011-2-1), and blood urea nitrogen (BUN, C013-2-1) biochemical test kits were purchased from Nanjing Jiancheng Bioengineering Institute (Nanjing, China). Enzyme-linked immunosorbent assay (ELISA) kits for glucose transporter 9 (GLUT9, RX201243M), ATP-binding cassette transporter G2 (ABCG2, RX200182M), urate transporter 1 (URAT1, RX200399M), occludin (RX202826M), and zonula occludens-1 (ZO-1, RX202825M) were obtained from Quanzhou Ruixin Biotechnology Co., Ltd. (Quanzhou, China). The Enhanced bicinchoninic acid assay (BCA) Protein Assay Kit, catalogued as P0010S, was sourced from Beyotime Biotechnology, headquartered in Shanghai, China.

Extraction of LTP from Poecilobdella manillensis lyophilized powder

First, *Poecilobdella manillensis* lyophilized powder was dissolved in phosphate-buffered saline (PBS) at a concentration of 39 mg/mL. The extraction was then performed using the ammonium sulfate saturation precipitation technique. Gradual ammonium sulfate salting-out stages were implemented to selectively harvest crude protein within the 30%-80% range. The procedural parameters are delineated in Supplementary Table 1. The protein activity of each fraction underwent meticulous examination. The methodology is outlined as follows: The solution was immersed in ammonium sulfate at 30% saturation, allowing it to rest in a refrigerated environment at 4 °C for 6 hours. Next, the solution underwent centrifugation at 8000 rpm for 20 minutes to remove precipitated impurities. These steps were repeated using 80% saturated ammonium sulfate, including centrifugation and harvesting of the resulting precipitate. The resolubilized and precipitated crude protein underwent further processing through centrifugal ultrafiltration, utilizing Millipore Amicon® Ultra 3KD tubes at 14000 rpm for 20 minutes, thereby facilitating ultrafiltration and desalination. The desalted crude protein solution (LTP) was meticulously amassed, appropriately concentrated, and stored at 4 °C[26-28].

Animals

Kunming mice (male, specific pathogen-free, 20-25 g) were provided by Tianqin Biotechnology Co., Ltd. (Changsha, China). Before the onset of the experimental procedures, all mice underwent a 1-week acclimation period in the designated animal facility, which was rigorously maintained at a temperature of 24 ± 2 °C, a humidity level of 50% ± 5%, and subjected to a 12 hours light/dark cycle. Throughout this preparatory phase, the subjects had unrestricted access to food and water, ensuring their physiological and psychological readiness for the forthcoming studies. All experimental procedures complied with the United Kingdom Animals (Scientific Procedures) Act 1986 and associated guidelines and

were approved by the Medical Ethics Committee of Guangxi University.

Animal treatment

For the induction of HUA and renal dysfunction, mice were provided with a high-purine diet and intraperitoneal injection of 200 μL PO for 7 consecutive days. The high-purine diet consisted of mice feedstuff (100 g), yeast extract (40 g), and yeast ribonucleic acid (2 g), which were re-granulated after melting the above ingredients. Potassium oxyate was dissolved in 0.5% sodium carboxymethyl cellulose solution at a concentration of 52.5 mg/mL.

In the study, 36 mice were randomly allocated into four parallel groups (8-10 mice in each group), comprising a normal control group (CON), a PO-induced HUA model group (HUA), a group treated with leech *Poecilobdella manillensis* total protein extract (LTP, receiving 49 mg/kg/day *via* intragastric administration), and a positive control group (AP, receiving 5 mg/kg/day AP by intragastric administration). The CON group was provided with a normal diet and intraperitoneal injection with 200 μL 0.5% sodium carboxymethyl cellulose, while the HUA group was provided with a high-purine diet and intraperitoneal injection with 200 μL PO. The modeling methods adopted by the LTP group and AP group were consistent with those of the HUA group. Animal modeling and pharmacotherapeutics commenced concurrently. The protein concentrations in the leech *Poecilobdella manillensis* lyophilized Powder and LTP were determined with the BCA method[29-32]. All groups of mice were anesthetized with isoflurane after the last pharmaceutical intervention. Urine and blood samples were collected to measure UA, CRE, and BUN. Hepatic tissue supernatant (detailed methods in "Detection of hepatic XOD activity" of Materials and Methods) was employed for the assessment of XOD. The supernatant derived from kidney and jejunum tissues was utilized for the evaluation of UA transporters, including URAT1, GLUT9, and ABCG2, in addition to the epithelial tight junction proteins ZO-1 and occludin.

Urinate collection

After 7 days of treatment, the mice were transferred to a clean and empty cage individually for the collection of urine, which was then centrifuged at 3500 rpm for 10 minutes. The supernatant was used for UA and CRE analyses directly.

Collection of serum and tissue samples

Animals were anesthetized using diethyl ether 1 hour after the last treatment, and blood was collected to obtain serum for the UA and CRE assays. Kidney and liver tissues were dissected quickly on ice and stored in liquid nitrogen for the following analyses.

Evaluation of UA, CRE, and BUN in the serum and urine

Blood and urine specimens were spun at 3500 rpm for 15 minutes at 4 °C to clear any sediment and extract the supernatant. UA concentrations were measured with an enzymatic colorimetric technique, as per the given guidelines. CRE levels were analyzed using a sarcosine oxidase-based CRE assay kit, following the provided instructions. Similarly, the level of BUN was assessed using a urea nitrogen assay kit following the urease method specified in the kit instructions.

Detection of hepatic XOD activity

To create a 10% liver homogenate, liver tissues were first washed with chilled PBS (0.01 mol/L, pH = 7.4) to eliminate residual blood. After weighing, the tissues were finely chopped on ice, and mixed with PBS at a specific ratio of 10 mg of tissue to 100 μL of PBS, effectively making 1 mL of buffer equivalent to 0.1 g of tissue. Protease inhibitors were added to the PBS to prevent protein degradation. The mixture was then homogenized using a pre-cooled tissue grinder. To further break down the tissue and cells, the homogenate underwent ultrasonication according to our experimental procedures. Following homogenization, the tissues were centrifuged at 7228 rpm for 8 minutes at -4 °C to separate the supernatant. Protein concentrations were quantified using an Enhanced BCA Protein Assay Kit. Liver XOD activity was then measured using an XOD test kit, according to the instructions.

Assessment of UA transporters and epithelial tight junction proteins

For the extraction of supernatant, tissue specimens were prepared by homogenizing jejunal and kidney tissues using a pre-cooled tissue grinder, as described above ("Detection of hepatic XOD activity"). Following homogenization, the tissues were spun at 7228 rpm for 8 minutes, and the supernatant was subsequently collected at -4 °C. The analysis of UA transporters (including URAT1, GLUT9, and ABCG2) and epithelial tight junction proteins (including ZO-1 and occludin) was performed using ELISAs, following the kit instructions.

Histological examination

Renal tissues were prepared for histological analysis using hematoxylin and eosin (HE) staining: (1) Fixation and embedding: Mouse kidney tissues were longitudinally sectioned, and immediately fixed in 4% paraformaldehyde. After 72 hours, the tissues were rinsed with running water for 15 minutes, dried with sterile gauze, and placed in dehydration trays; (2) Dehydration: Tissues underwent dehydration using an increasing series of ethanol concentrations in a dehydration device. This included 75% ethanol for 4 hours, followed by 85% for 2 hours, and then 90%, 95%, and absolute ethanol stages I and II for 1.5 hours, 1 hour, and 30 minutes, respectively; (3) Clearing and infiltration: Post-dehydration, the tissues underwent clearing in xylene, which facilitates better paraffin infiltration due to its miscibility with both ethanol and paraffin. Subsequently, the tissues were infiltrated using a graded series of paraffin wax at 60 °C to ensure complete penetration; (4) Sectioning: The embedded tissues were sectioned at 4 μm thickness using a microtome, floated in a 40 °C water bath for expansion, and mounted on adhesion slides. The slides were then dried in a 60 °C oven for 3

hours to adhere the sections; and (5) Staining: (a) Deparaffinization: Sections were deparaffinized in xylene and rehydrated through a graded series of ethanol to water; (b) Staining: Sections were stained in Mayer's hematoxylin for 5 minutes, washed, and differentiated in 1% hydrochloric acid in ethanol for 2-3 seconds. After rinsing, sections were blued in 0.6% ammonia water and then stained with 1% aqueous eosin for 5 minutes; and (c) Dehydration and clearing: Ultimately, sections underwent dehydration in alcohol, were cleared using xylene, and were mounted in neutral resin for microscopic analysis.

Untargeted metabolomics analysis using ultra-high performance liquid chromatography with quadrupole time-of-flight mass spectrometry

Metabolomics instrument: Q-Exactive Quadrupole-Orbitrap High-Resolution Mass Spectrometer (Thermo Scientific, United States), UltiMate 3000 Ultra High-Performance Liquid Chromatography System (Thermo Scientific, United States).

Chromatography conditions: The chromatographic analysis employed an ACQUITY UPLC BEH C18 column with dimensions of 50 mm by 2.1 mm and a particle size of 1.7 μm. The column was kept at a constant 30 °C, while the autosampler was cooled to 10 °C. For both positive and negative ion modes, the mobile phases were 0.1% formic acid in water (Phase A) and methanol (Phase B). The gradient elution was structured as follows: From 0 to 2 minutes, 95% Phase A; over the next 11 minutes, decreased linearly to 0% Phase A; held at 0% Phase A from 13 to 16 minutes; rapidly reverted to 95% Phase A within 0.1 minutes; and held at 95% Phase A from 16.1 to 19 minutes. The chromatography utilized a flow rate of 0.3 mL/min and an injection volume of 2 μL.

Mass spectrometry conditions: Ionization used a heated electrospray source at 350 °C. The spray voltage for negative ion mode was 3.0 kV. The transfer capillary temperature was at 320 °C, the sheath gas pressure was 35 psi, and the auxiliary gas flow was 10 psi. Full mass scan (MS) and data-dependent MS/MS scan mode was used, covering a mass range of 200 to 2000 m/z. Resolutions were 70000 for first-stage and 17500 for second-stage scans, with high-purity nitrogen as the collision gas.

Workflow for cecal microbiota analysis

Cecal content specimens were procured from the cecal regions. Genomic DNA was extracted employing the Cetyltrimethylammonium Bromide methodology[33]. After extraction, the concentration and purity of the DNA were meticulously evaluated *via* electrophoresis conducted on a 1% agarose gel, a standard procedure to ensure the integrity and quality of the genetic material for downstream applications. This step is crucial in molecular biology workflows to ascertain the suitability of DNA samples for further analyses. Following the assessment, DNA was diluted to a standard concentration of 1 ng/μL utilizing a sterile aqueous solution for the amplification process.

Amplification of the 16S rRNA gene sequences, specifically targeting the V3-V4 regions, was achieved using primers 341F (5'-CCTAYGGGRBGCASCAG-3') and 806R (5'-GGACTACNNGGGTATCTAAT-3'), each appended with a unique barcode. The polymerase chain reaction (PCR) amplifications were executed within a reaction volume of 15 μL, incorporating Phusion® High-Fidelity PCR Master Mix, sourced from New England Biolabs, Beijing, China. This reaction mixture also included 2 μmol/L concentrations of both the forward and reverse primers, alongside an approximate 10 ng quantity of template DNA. The thermal cycling protocol was initiated with a denaturation phase at 98 °C for 1 minute. This phase was succeeded by 30 cycles, each comprising a denaturation step at 98 °C for 10 seconds, an annealing step at 50 °C for 30 seconds, and an elongation step at 72 °C for 30 seconds. The cycling protocol was finalized with an elongation phase at 72 °C, extending for 5 minutes, to ensure the completion of DNA synthesis. This methodological approach ensures the fidelity and specificity of the amplified DNA sequences, which is integral for subsequent molecular analyses.

Following amplification, the PCR products underwent electrophoresis within a 2% agarose gel matrix, utilizing a 1X Tris-acetate-EDTA buffer, to evaluate the results of amplification. Subsequently, PCR products were pooled at equimolar concentrations and the pooled products were purified using the Universal DNA Purification Kit (TianGen, Beijing, China). The generation of sequencing libraries was meticulously conducted utilizing the NEB Next® Ultra DNA Library Prep Kit (Illumina, headquartered in San Diego, United States), adhering stringently to the guidelines provided by the manufacturer. Following library preparation, index codes were appended to facilitate the identification and multiplexing of samples. The assessment of library integrity and quality was performed using the Agilent 5400 Bioanalyzer (Agilent Technologies, California, United States), ensuring optimal library standards before sequencing. Upon satisfactory evaluation of library quality, sequencing was undertaken on the Illumina sequencing platform. This process yielded 250 bp paired-end reads, allowing for comprehensive coverage and depth of the genomic regions.

Bioinformatics and statistical analysis

Bioinformatics analysis of the gut microbiome: Bioinformatics analysis followed the "Atacama Soil Microbiome Tutorial" from Qiime2docs, supplemented with custom scripts. Raw FASTQ data were imported into QIIME2, then underwent quality control, trimming, denoising, and chimeric sequence removal using the dada2 plugin, resulting in an amplicon sequence variant feature table. The taxonomic classification used the GREENGENES 13_8 99% Operational Taxonomic Unit database, with V3-V4 region alignment *via* QIIME2 plugins, excluding mitochondrial and chloroplast DNA. Statistical tools, including ANCOM, ANOVA, and DESeq2, were used to identify differentially abundant bacteria across samples. Microbial diversity within samples (alpha diversity) and between samples (beta diversity) was assessed using QIIME2 indices and was visualized through principal coordinate analysis (PCoA). Partial least squares discriminant analysis (PLS-DA), through "mixOmics" and "vegan" R packages, respectively, explored the impact of microbiota variations and environmental factors. Spearman's rank correlations highlighted taxa associations, visualized in network plots. Functional predictions of microbial communities were estimated with Phylogenetic Investigation of

Communities by Reconstruction of Unobserved States, adhering to default parameters for consistent and reproducible analysis, in line with top-tier microbiome research standards.

Metabolomics data processing and analysis: Data processing was conducted using CD 3.1 software for peak detection, alignment, and normalization based on retention times and m/z values, forming two-dimensional data matrices. These were analyzed in MetaboAnalyst 6.0 for pattern recognition, employing the 80% rule to refine data for statistical evaluation. PLS-DA and orthogonal PLS-DA (OPLS-DA) methods were pivotal in variance analysis and identifying metabolomic differences between groups, with validation through permutation tests and K-fold cross-validation. VIP scores from OPLS-DA, indicating significant metabolite contributions, guided the identification of differential metabolites with VIP > 1, $P < 0.05$, and significant fold changes (FC), FC ≥ 1.5, or FC ≤ 0.67.

Differential metabolites were identified using the Human Metabolome Database and METLIN databases, ensuring accuracy by matching molecular mass and ionization details closely with experimental data. This facilitated the elucidation of metabolites linked to HUA. MetaboAnalyst 6.0 further explored the metabolic pathways affected by these metabolites, visualizing pathway impact and significance through bubble charts, and highlighting pathways with $P < 0.05$ as significantly altered. This comprehensive approach provided insights into the metabolites' roles and their implications in HUA, enhancing the understanding of the condition's metabolic underpinnings. PLS-DA, PCoA, and O2-PLS models were used to integrate the metabolome and microbiome datasets, which are described in detail above. The model was calculated on paired data sets; significant variables were then selected based on their correlation with the model score ($P < 0.01$).

Analysis of non-omics data: For numerical variables adhering to a normal distribution, descriptive statistics were articulated as means with standard deviations. Group comparisons were conducted using the *t*-test for two groups and ANOVA for more than two groups. Upon detecting significant differences between groups, the least significant difference technique was applied for subsequent pairwise comparisons. In instances where the assumption of normality was violated, descriptive statistics were presented as medians accompanied by interquartile ranges. Comparative analysis between two independent samples was conducted using the Mann-Whitney *U* test, whereas the Kruskal-Wallis *H* test facilitated comparisons across multiple groups. Upon identifying statistically significant disparities among groups, the Dunn's Sidak-Correction Factor method was employed for *post-hoc* multiple comparisons.

RESULTS

LTP ameliorated disruptions in UA and renal function in PO-induced HUA mice

The effect of LTP in terms of lowering urate was investigated in HUA mice. After 7 days of modeling, the HUA mice had considerably higher serum and urine UA and XOD levels than mice in the CON group, demonstrating that the HUA mouse model had been successfully constructed (Figure 1A-C). Compared with the HUA mice, mice in the LTP and AP groups had significantly decreased serum levels of UA ($P < 0.0001$) and liver XOD activity ($P < 0.01$) (Figure 1A and C). To assess renal function in HUA mice, serum CRE and BUN levels were analyzed. Serum CRE levels were significantly increased in the HUA mice, which were decreased by LTP ($P < 0.05$) (Figure 1D). Serum BUN levels showed a decreasing trend; however, this was not statistically significant between groups (Figure 1E). HE staining highlighted the differences in the renal morphology among the groups. The CON group exhibited well-organized tubules, clear lumens, and intact glomeruli. In contrast, the HUA model group showed severe renal damage, including tubular swelling, atrophy, and disordered epithelial alignment with disrupted glomeruli, in addition to pronounced inflammatory infiltration and vascular congestion. The LTP and AP treatment groups demonstrated significant protective effects; LTP notably reduced inflammation and restored the renal structure to that closely resembling the CON group, while AP was slightly less effective in alleviating congestion and glomerular changes (Figure 1F).

LTP promoted UA excretion by modulating urate transporters

Urate transporters are mainly responsible for UA excretion. Compared with the CON group, the concentrations of the renal tissue reabsorption transporters URAT1 and GLUT9 were elevated in the HUA group, while the concentration of the renal tissue secretory transporter ABCG2 was decreased in the HUA group. Following interventions with LTP and AP, reversals of these observations were seen in the LTP and AP groups (Figure 2A-C). Similarly, the concentrations of URAT1 and GLUT9 were upregulated in the jejunal tissues of the HUA group compared to the CON group, and there were decreases in URAT1 and GLUT9 after LTP treatment; however, these differences were not statistically significant (Figure 2D and E). The trend of ABCG2 expression in jejunal tissue was consistent with that in renal tissue (Figure 2F).

LTP ameliorated renal and intestinal barrier impairment in HUA mice

Epithelial tight junction proteins in renal and jejunal tissues were assessed to further investigate the extent of renal and intestinal barrier impairment. Compared with the CON group, the concentrations of the renal tissue epithelial tight junction proteins ZO-1 and occludin were decreased in the HUA group ($P < 0.05$) (Figure 3A and B). However, following treatment with LTP and AP, the concentrations of ZO-1 and occludin in renal tissues showed an increasing trend ($P < 0.01$) (Figure 3A and B). The concentrations of ZO-1 and occludin in jejunum tissue showed a similar trend as in renal tissue. Notably, the increase in jejunal tissue ZO-1 was statistically significant only in the LTP group ($P < 0.05$), whereas there was no statistically significant difference in the AP group ($P = 0.062$) (Figure 3C and D).

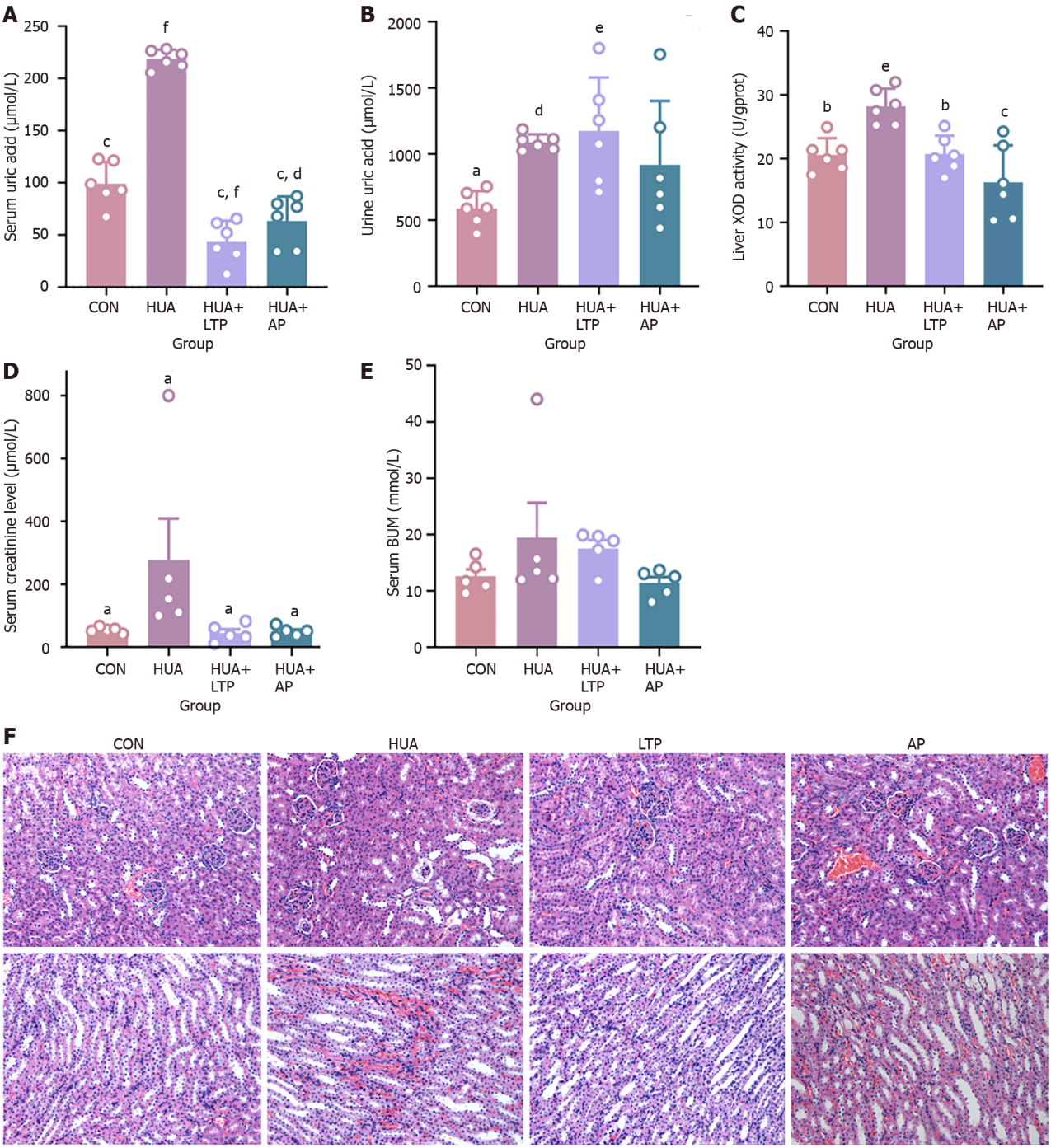

Figure 1 Effect of leech *Poecilobdella manillensis* total protein extract treatment on hyperuricemia. A: Serum uric acid levels; B: Urine uric acid levels; C: Liver xanthine oxidase activity; D: Serum creatinine levels; E: Blood urea nitrogen levels; F: Renal tissue hematoxylin and eosin staining pathology under 200 × magnification. Statistical significance determined by ANOVA is indicated as follows: $^{a}P < 0.05$ *vs* hyperuricemia model group (HUA); $^{b}P < 0.01$ *vs* HUA; $^{c}P < 0.001$ *vs* HUA; $^{d}P < 0.05$ *vs* normal control group (CON); $^{e}P < 0.01$ *vs* CON; $^{f}P < 0.001$ *vs* CON. CON: Normal control group; HUA: Hyperuricemia model group; AP: Allopurinol treatment group; LTP: Leech *Poecilobdella manillensis* total protein extract treatment group; XOD: Xanthine oxidase; BUN: Blood urea nitrogen.

LTP remodeled gut microbiota composition in HUA mice

To further analyze the UA-lowering potential of LTP, cecum content samples were subjected to 16S rRNA gene sequencing. Cecum microbiota communities were profiled using 16S rRNA gene V3-V4 pyrosequencing. The amount of sequencing data was sufficient to cover almost all micro-organisms, judging from the alpha rarefaction curve of all samples (Supplementary Figure 1A and B). First, the α diversity (including Shannon and Simpson indices) and β diversity were used to analyze the differences in microbial diversity within and between groups. The Shannon and Simpson indices in the HUA group were lower when compared to the CON group. However, the above indices in the LTP group were higher than those in the HUA group, with the results for Shannon's index being statistically different ($P < 0.05$) (Figure 4A and B), suggesting that LTP could improve the richness and diversity of the gut microbiota in HUA mice. To assess the differences in gut microbial composition, PCoA and PLS-DA were performed. The PLS-DA analysis showed that the cluster of the HUA group was separated from that of the CON and LTP groups (Figure 4C, Supplementary

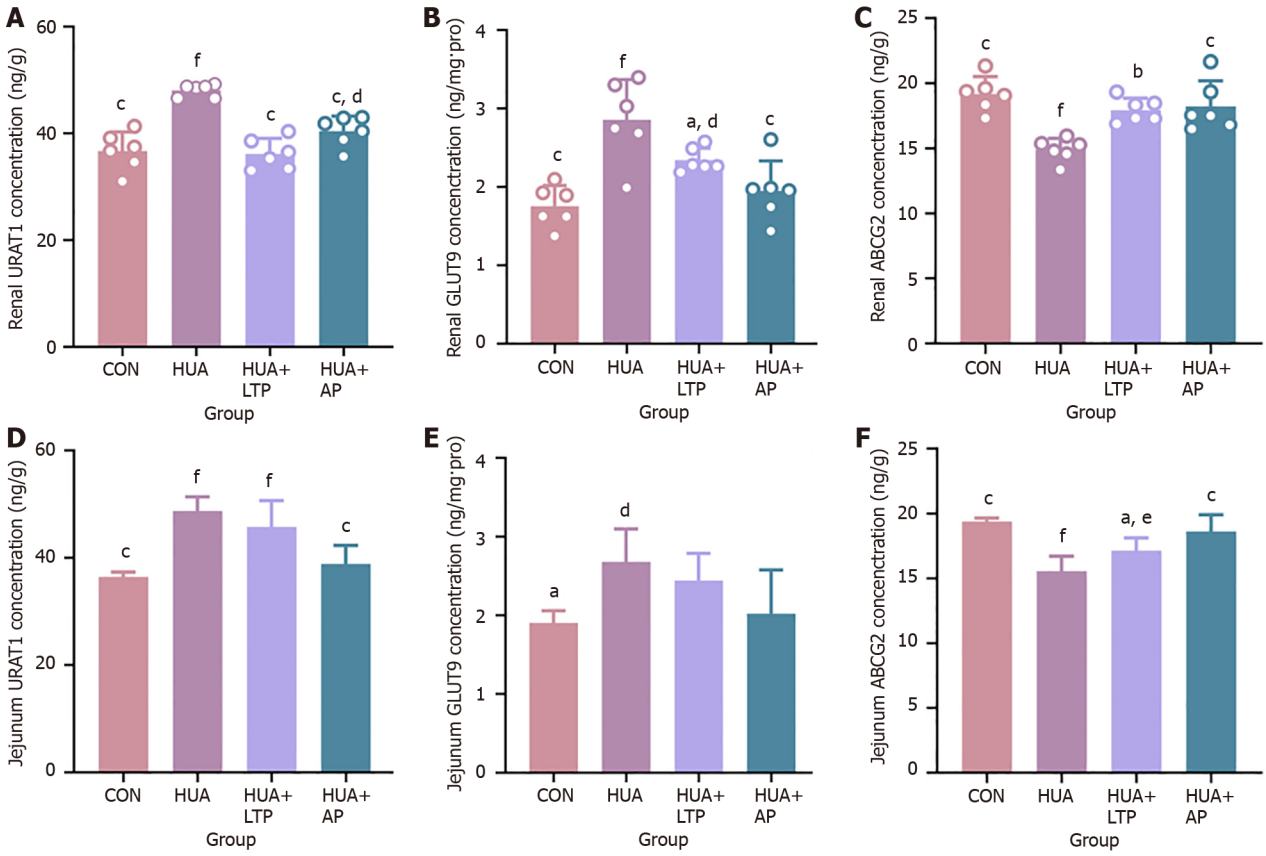

Figure 2 Effect of leech *Poecilobdella manillensis* total protein extract on facilitating uric acid excretion, evaluated by enzyme-linked immunosorbent assay. A: Renal urate transporter 1 (URAT1) concentration level; B: Renal glucose transporter 9 (GLUT9) concentration level; C: Renal ATP-binding cassette transporter G2 (ABCG2) concentration level; D: Jejunum URAT1 concentration level; E: Jejunum GLUT9 concentration level; F: Jejunum ABCG2 concentration level. Statistical significance determined by ANOVA is indicated as follows: $^{a}P < 0.05$ *vs* hyperuricemia model group (HUA); $^{b}P < 0.01$ *vs* HUA; $^{c}P < 0.001$ *vs* HUA; $^{d}P < 0.05$ *vs* normal control group (CON); $^{e}P < 0.01$ *vs* CON; $^{f}P < 0.001$ *vs* CON. Sample sizes: Renal tissue $n = 6$ for each group; Jejunum tissue $n = 4$ for each group. CON: Normal control group; HUA: Hyperuricemia model group; AP: Allopurinol treatment group; LTP: Leech *Poecilobdella manillensis* total protein extract treatment group; URAT1: Urate transporter 1; GLUT9: Glucose transporter 9; ABCG2: ATP-binding cassette transporter G2.

Figure 1C). PCoA plots showed that the cluster of the CON group was separated from that of the HUA group, while the LTP group was partially separated from the HUA group, and there was a significant difference ($P < 0.01$) among the three groups, as analyzed using permanova statistics (Figure 4D, Supplementary Figure 1D-G), indicating that LTP treatment altered the composition and distribution of the gut microbiota in HUA mice.

At the phylum level, the gut microbiome was dominated by *Firmicutes*, *Bacteroidota*, *Proteobacteria*, *Desulfobacterota*, *Verrucomicrobiota*, *Campilobacterota*, and *Patescibacteria*, which differed among the CON, HUA, and LTP groups (Figure 4E). Compared with the CON group, HUA group mice had a lower ratio of *Firmicutes* to *Bacteroidota* (F/B). After LTP treatment, the F/B ratio was significantly higher (Figure 5A), restoring gut microbial abundance and showing a similar microbial distribution to the CON group. The structural changes in the gut microbiota at the genus level were studied (Figures 4F and 5A-C). The absolute abundances of *Lactobacillus*, *Clostridium_sensu_stricto_1*, *Bifidobacterium*, *Prevotella*, and *Escherichia_Shigella* in the HUA group were remarkably lower than those in the CON group, while *Bacteroides*, *Alloprevotella*, and *Sphingomonas* were significantly enriched in the HUA group. LTP treatment reversed these changes and remodeled the bacterial abundance similar to that in the CON group. In addition, the LTP group showed a specific increase in the abundance of *Enterococcus*, *Dialister*, *Delftia*, *Faecalibacterium*, and *Akkermansia* (Figure 5A-C). Linear discriminant analysis effect size (LEfSe) analysis was used to compare the differences between the three groups at the phylum and genus level; with the threshold of the logarithmic linear discriminant analysis score as 4.0 and $P < 0.01$, it revealed that *Firmicutes*, *Bacteroidota*, *Proteobacteria*, and *Verrucomicrobiota* were significantly different species at the phylum level (Figure 4G). The LEfSe analysis also revealed that the abundance of *Bacteroides*, *Akkermansia*, *Escherichia_Shigella*, *Prevotella*, *Sphingomonas*, *Parabacteroides*, and *Alloprevotella* in the HUA and LTP groups significantly differed at the genus level (Figure 4H). Collectively, these results indicate that LTP modulated the gut microbiota of HUA mice, thereby alleviating PO-induced microecological dysregulation. Based on the Phylogenetic Investigation of Communities by Reconstruction of Unobserved States, the possible functions of the altered gut microbiota (CON *vs* HUA and HUA *vs* LTP) were analyzed. Figure 4I and J show the primary metabolic pathways with significant differences ($P < 0.05$).

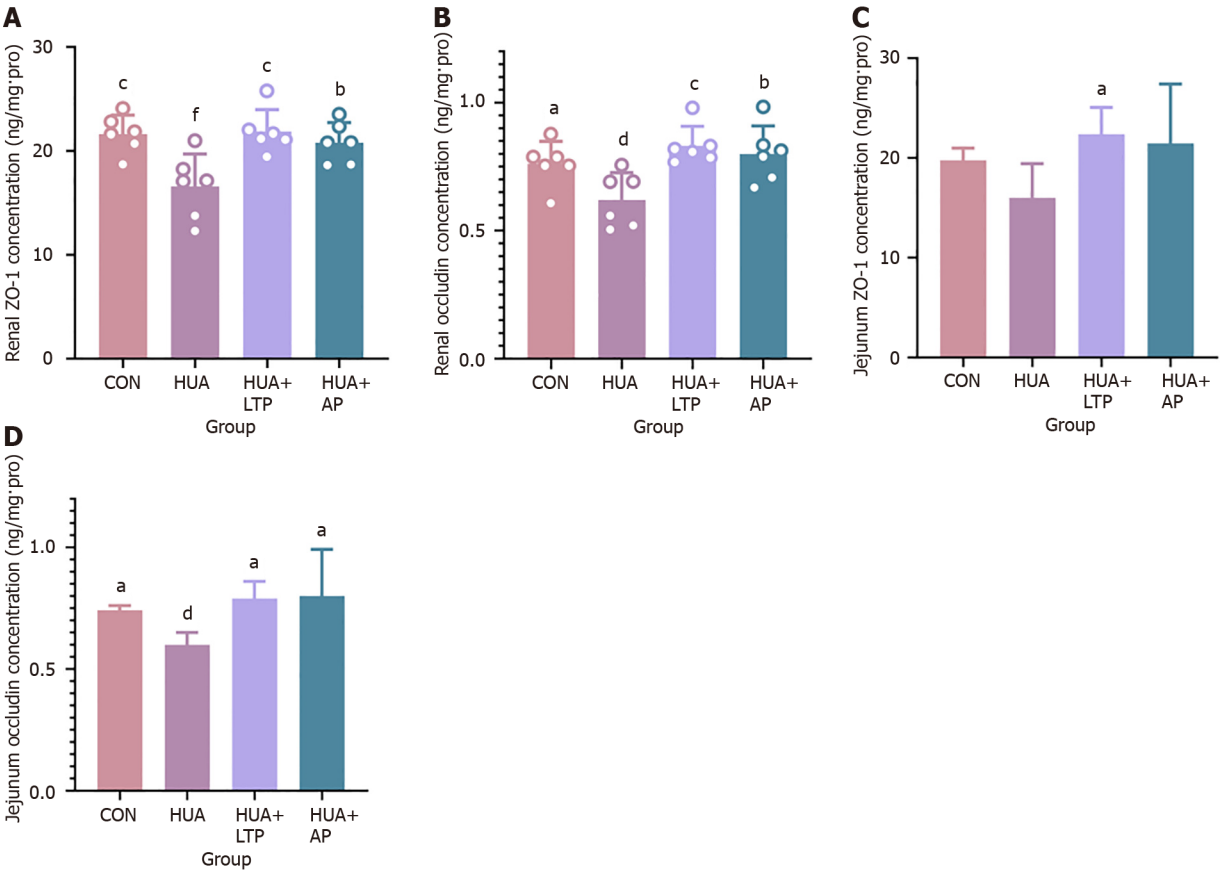

Figure 3 Effect of leech *Poecilobdella manillensis* total protein extract on epithelial tight junction proteins, evaluated by enzyme-linked immunosorbent assay. A: Renal zonula occludens-1 (ZO-1) concentration level; B: Renal occludin concentration level; C: Jejunum ZO-1 concentration level; D: Jejunum occludin concentration level. Statistical significance determined by ANOVA is indicated as follows: $^{a}P < 0.05$ *vs* hyperuricemia model group (HUA); $^{b}P < 0.01$ *vs* HUA; $^{c}P < 0.001$ *vs* HUA; $^{d}P < 0.05$ *vs* normal control group (CON); $^{f}P < 0.001$ *vs* CON. Sample sizes: Renal tissue $n = 6$ for each group; Jejunum tissue $n = 4$ for each group. CON: Normal control group; HUA: Hyperuricemia model group; AP: Allopurinol treatment group; LTP: Leech *Poecilobdella manillensis* total protein extract treatment group; ZO-1: Zonula occludens-1.

LTP altered the serum metabolite composition in PO-induced HUA mice

We analyzed the serum metabolic profiles using ultra-high performance liquid chromatography with quadrupole time-of-flight mass spectrometry. The results of the PLS-DA score plot showed that the quality control samples were well-clustered in both positive and negative ion modes (Supplementary Figure 2A-F), indicating that the analytical method had good stability and reliability, which could be applied for the subsequent analysis of serum metabolites. As shown in the PLS-DA score plot (Figure 6A and B, Supplementary Figure 2G and H), the HUA and CON groups were separated, indicating significant differences in the metabolites of the two groups of mice. The LTP group and HUA group were separated, indicating that the LTP treatment could regulate the PO-induced alterations in serum metabolites. On the other hand, OPLS-DA was applied to further identify potential biomarkers with significant changes in concentration. The OPLS-DA results indicated a significant trend of separation in pairwise comparisons between CON and HUA groups, as well as between HUA and LTP groups (Figure 6C-F). As shown in Supplementary Table 2, using the criteria of VIP > 1 and FC ≤ 0.67 or ≥ 1.50, we screened a total of 98 common differential metabolites. The volcano map shows changes in serum metabolites between the HUA and CON groups; supplementation with LTP not only partially reversed some of these changes induced by HUA but also introduced new alterations in the serum metabolites (Figure 6G and H).

In total, 22 potential biomarkers were discovered by consulting both the Human Metabolome Database and the Kyoto Encyclopedia of Genes and Genomes (KEGG) database, as outlined in Supplementary Table 3. Heatmaps were generated to demonstrate global trends in differential metabolites between groups (Figure 7A). Sphinganine, D-glucose, L-tyrosine, ophthalmic acid, arachidonic acid, docosahexaenoic acid, 20-hydroxyeicosatetraenoic acid, and 8,11,14-eicosatrienoic acid were significantly increased in the HUA group compared to the CON group, while stearic acid and 5′-methylthioadenosine were significantly decreased. LTP treatment significantly reversed the changes in the above metabolites (Figure 7B). Further, KEGG pathway analysis of differential metabolites revealed that sphingolipid metabolism, tyrosine metabolism, primary bile acid biosynthesis, steroid hormone biosynthesis, starch and sucrose metabolism, galactose metabolism, and purine metabolism were significantly altered in the HUA group when compared with the CON group; while LTP significantly modulated cysteine and methionine metabolism, starch and sucrose metabolism, sphingolipid metabolism, galactose metabolism, and phenylalanine, tyrosine, and tryptophan biosynthesis, when compared with the HUA group (Figure 6I and J).

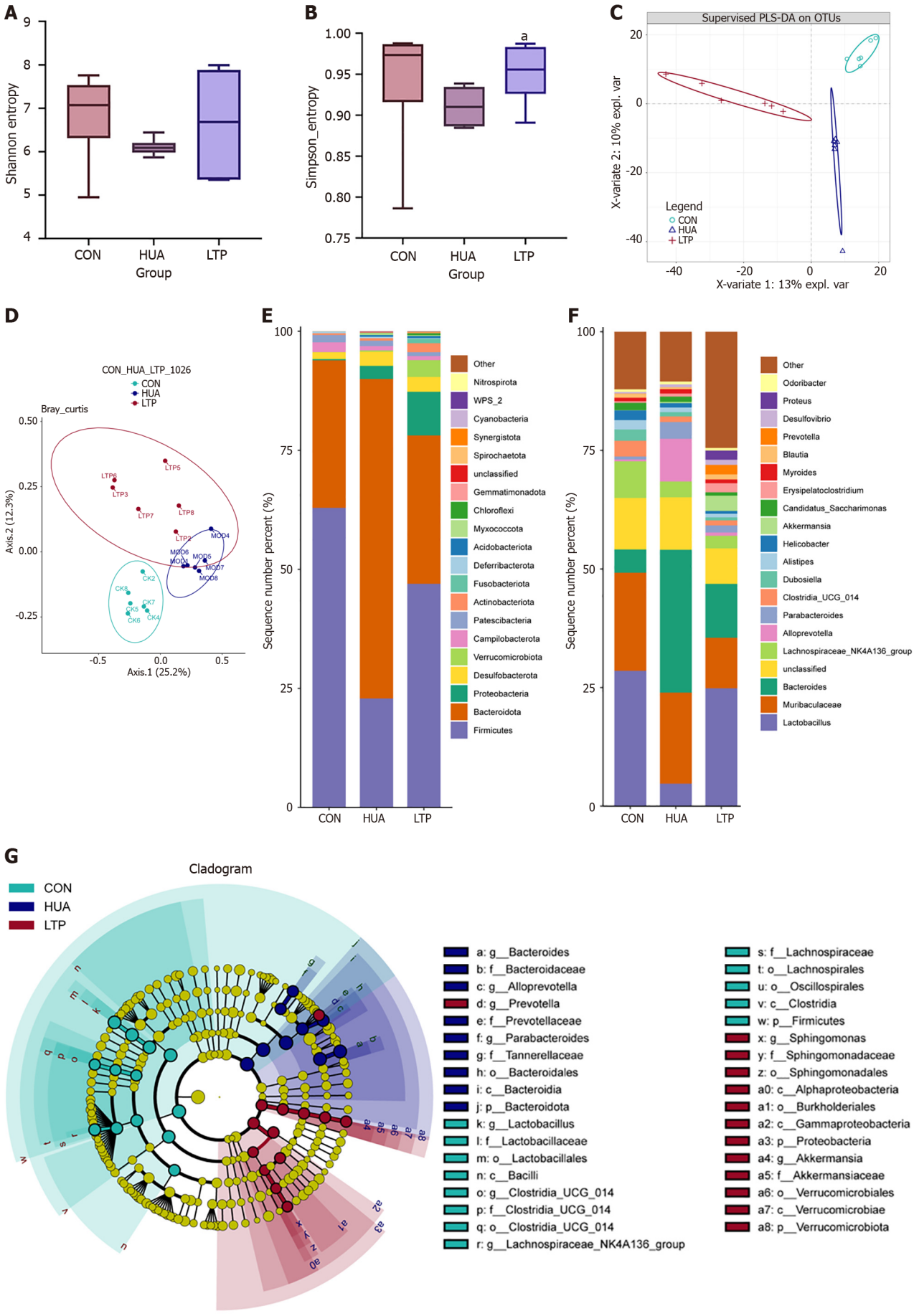
A
Shannon entropy
CON
HUA
LTP
Group
B
Simpson_entropy
a
CON
HUA
LTP
Group
C
Supervised PLS-DA on OTUs
X-variate 2: 10% expl. var
X-variate 1: 13% expl. var
Legend
CON
HUA
LTP
D
CON_HUA_LTP_1026
CON
HUA
LTP
Bray_curtis
Axis.2 (12.3%)
Axis.1 (25.2%)
E
Sequence number percent (%)
Other
Nitrospirota
WPS_2
Cyanobacteria
Synergistota
Spirochaetota
unclassified
Gemmatimonadota
Chloroflexi
Myxococcota
Acidobacteriota
Deferribacterota
Fusobacteriota
Actinobacteriota
Patescibacteria
Campilobacterota
Verrucomicrobiota
Desulfobacterota
Proteobacteria
Bacteroidota
Firmicutes
F
Sequence number percent (%)
Other
Odoribacter
Proteus
Desulfovibrio
Prevotella
Blautia
Myroides
Erysipelatoclostridium
Candidatus_Saccharimonas
Akkermansia
Helicobacter
Alistipes
Dubosiella
Clostridia_UCG_014
Parabacteroides
Allprevotella
Lachnospiraceae_NK4A136_group
unclassified
Bacteroides
Muribaculaceae
Lactobacillus
G
Cladogram
CON
HUA
LTP
a: g__Bacteroides
b: f__Bacteroidaceae
c: g__Alloprevotella
d: g__Prevotella
e: f__Prevotellaceae
f: g__Parabacteroides
g: f__Tannerellaceae
h: o__Bacteroidales
i: c__Bacteroidia
j: p__Bacteroidota
k: g__Lactobacillus
l: f__Lactobacillaceae
m: o__Lactobacillales
n: c__Bacilli
o: g__Clostridia_UCG_014
p: f__Clostridia_UCG_014
q: o__Clostridia_UCG_014
r: g__Lachnospiraceae_NK4A136_group
s: f__Lachnospiraceae
t: o__Lachnospirales
u: o__Oscillospirales
v: c__Clostridia
w: p__Firmicutes
x: g__Sphingomonas
y: f__Sphingomonadaceae
z: o__Sphingomonadales
a0: c__Alphaproteobacteria
a1: o__Burkholderiales
a2: c__Gammaproteobacteria
a3: p__Proteobacteria
a4: g__Akkermansia
a5: f__Akkermansiaceae
a6: o__Verrucomicrobiales
a7: c__Verrucomicrobiae
a8: p__Verrucomicrobiota

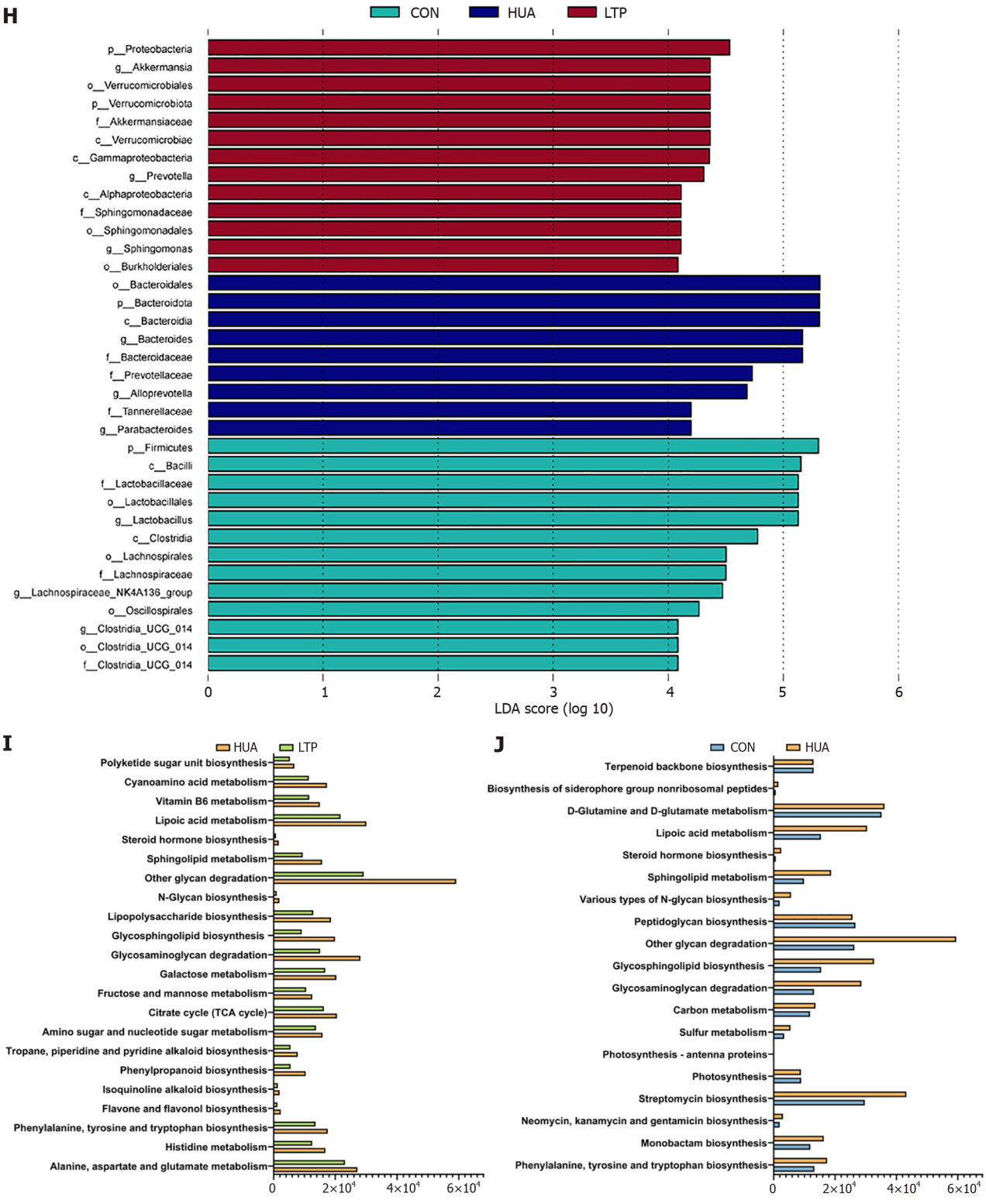

Figure 4 Leech *Poecilobdella manillensis* total protein extract alters the gut microbiota in potassium oxonate-induced hyperuricemia mice. A: Shannon index across three groups; B: Simpson index across three groups; C: Partial least squares discriminant analysis of three groups; D: Principal coordinate analysis of three groups; E: Distribution plot of relative abundance at the phylum level of bacteria; F: Distribution plot of relative abundance at the genus level of bacteria; G: Cladogram from linear discriminant analysis effect size (LEfSe) analysis identifying highly differentiated taxa from phylum to genus levels; H: Linear discriminant analysis graph from LefSe analysis identifying highly differentiated taxa from phylum to genus levels; I: Predicted functional pathways of gut microbiota in hyperuricemia model group (HUA) *vs* leech *Poecilobdella manillensis* total protein extract treatment group; J: Predicted functional pathways of gut microbiota in normal control group *vs* HUA. Statistical significance is indicated as follows: $^{a}P < 0.05$ *vs* hyperuricemia model group. Sample size: $n = 6$ per group. CON: Normal control group; HUA: Hyperuricemia model group; LTP: Leech *Poecilobdella manillensis* total protein extract treatment group; LDA: Linear discriminant analysis.

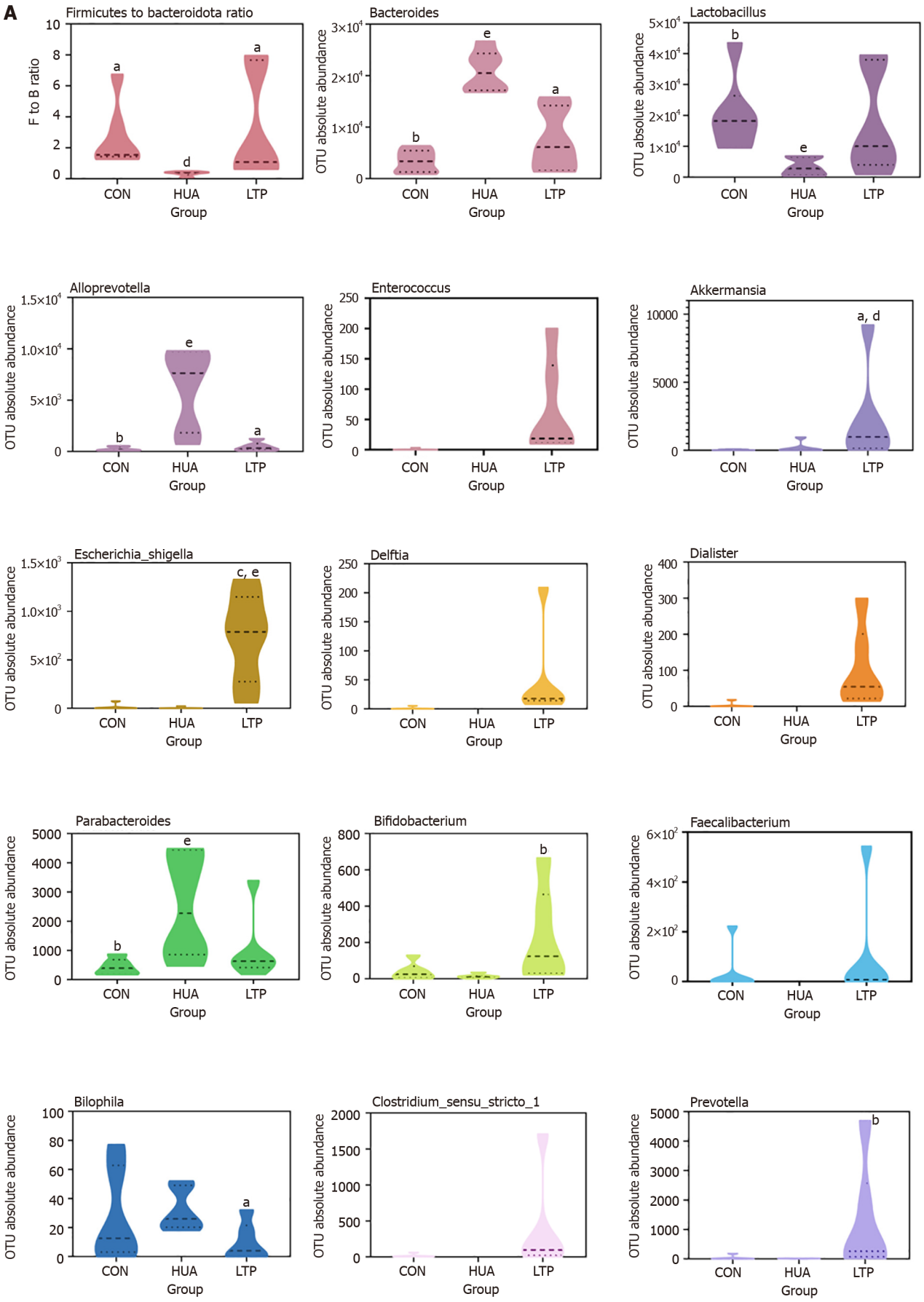
A
Firmicutes to bacteroidota ratio
F to B ratio
Bacteroides
OTU absolute abundance
Lactobacillus
Alloprevotella
Enterococcus
Akkermansia
Escherichia_shigella
Delftia
Dialister
Parabacteroides
Bifidobacterium
Faecalibacterium
Bilophila
Clostridium_sensu_stricto_1
Prevotella
CON
HUA
LTP
Group

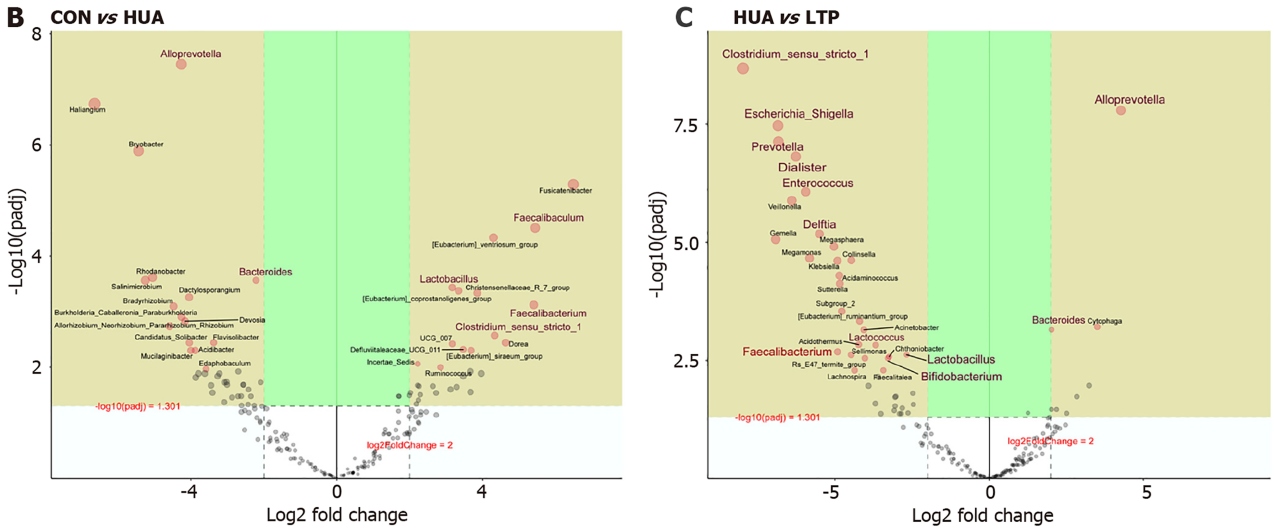

Figure 5 Effect of leech *Poecilobdella manillensis* total protein extract on vital microbial genus. A: The absolute abundance of vital microbial genera in all groups, assessed through the Kruskal-Wallis ANOVA; B and C: Significant differences between each two groups at the genus level of gut microbiota, determined by DESeq2 method [B: normal control group *vs* hyperuricemia model group (HUA); C: HUA *vs* leech *Poecilobdella manillensis* total protein extract treatment group; $n = 6$ for each group]. Statistical significance is indicated as follows: $^{a}P < 0.05$ *vs* hyperuricemia model group (HUA); $^{b}P < 0.01$ *vs* HUA; $^{c}P < 0.001$ *vs* HUA; $^{d}P < 0.05$ *vs* normal control group (CON); $^{e}P < 0.01$ *vs* CON. CON: Normal control group; HUA: Hyperuricemia model group; LTP: Leech *Poecilobdella manillensis* total protein extract treatment group.

Correlation analysis between the gut microbiota and metabolites

When integrating the results of the microbiome and metabolome analysis, we found that the sphingolipid metabolism and galactose metabolism pathways coexisted in both the microbiota and metabolome (Figures 4I and J, 6I and J). To further elucidate the influential gut microbiota in the metabolite alterations from all groups, Pearson correlation analysis was employed to explore potential associations between gut bacterial composition and host metabolites (Supplementary Figure 3, Supplementary Tables 4 and 5). The findings indicated a substantial relationship between the LTP regulatory effects on metabolites and the abundance of *Bacteroides*, *Enterococcus*, *Faecalibacterium*, *Alloprevotella*, *Prevotellaceae_UCG_001*, *Lactococcus*, *Dialister*, *Delftia*, *Clostridium_sensu_stricto_1*, *Escherichia_Shigella*, *Dialister*, *Akkermansia*, and *Prevotella* (Figure 8). In particular, sphinganine - a metabolite within the sphingolipid metabolic pathway - exhibited significant negative correlations with *Delftia*, *Dialister*, *Clostridium_sensu_stricto_1*, *Escherichia_Shigella*, *Enterococcus*, and *Prevotella*, while indicating a notable positive correlation with *Bacteroides*. Furthermore, D-glucose - a metabolite within the galactose metabolism pathway - exhibited significant negative correlations with *Escherichia_Shigella*, *Akkermansia*, *Lactococcus*, *Enterococcus, Delftia*, *Dialister*, and *Prevotella*, while indicating a notable positive correlation with *Bacteroides* (Figure 8, Supplementary Tables 6 and 7). In conclusion, alterations in metabolites following LTP treatment were found to be intricately correlated with the regulation of gut microbiota, specifically *Prevotella*, *Delftia*, *Dialister*, *Akkermansia*, *Lactococcus*, *Escherichia_Shigella*, *Enterococcus*, and *Bacteroides*. Furthermore, LTP exhibited the potential to ameliorate HUA by modulating gut microbiome-dependent metabolism within the sphingolipid metabolic and galactose metabolic pathways.

Correlation analysis between gut microbiota and HUA-related parameters

To examine the relationship between the gut microbiome and HUA-related biochemical indicators, urate transporters, and epithelial tight junction proteins, the Pearson correlation coefficients were investigated. *Bifidobacterium*, *Clostridium_sensu_stricto_1*, *Enterococcus*, *Delftia*, *Escherichia_Shigella*, *Prevotella*, *Dialister*, and *Faecalibaculum* displayed strong negative correlations with serum UA and serum CRE ($P < 0.05$), while *Bacteroides*, *Alloprevotella*, *Bilophila*, and *Bryobacter* showed strong positive correlations with serum UA and serum CRE ($P < 0.01$). *Delftia*, *Enterococcus*, *Lactococcus*, and *Dialister* displayed strong negative correlations with liver XOD concentration ($P < 0.01$), while *Bryobacter*, *Alloprevotella*, and *Bacteroides* displayed strong positive correlations with hepatic XOD concentration ($P < 0.01$). The results of the correlation analysis demonstrated that the absolute abundance levels of *Delftia*, *Enterococcus*, *Enterococcus*, *Clostridium_sensu_stricto_1*, *Escherichia_Shigella*, *Prevotella*, *Dialister*, *Alloprevotella*, and *Bacteroides* were closely related to the changes in renal and intestinal urate transporters and epithelial tight junction proteins. This suggests that the above gut microbiota contributed to the occurrence and recovery of HUA (Figure 9, Supplementary Table 8 and 9).

DISCUSSION

HUA has become a public health concern that needs to be solved urgently. Many of the previous studies have focused on the therapeutic effects of hirudin[24,25]; however, the associated mechanism has not been clarified, and no experiments on the reduction of UA by LTP have been reported. Based on verification of the effectiveness of *Poecilobdella manillensis*

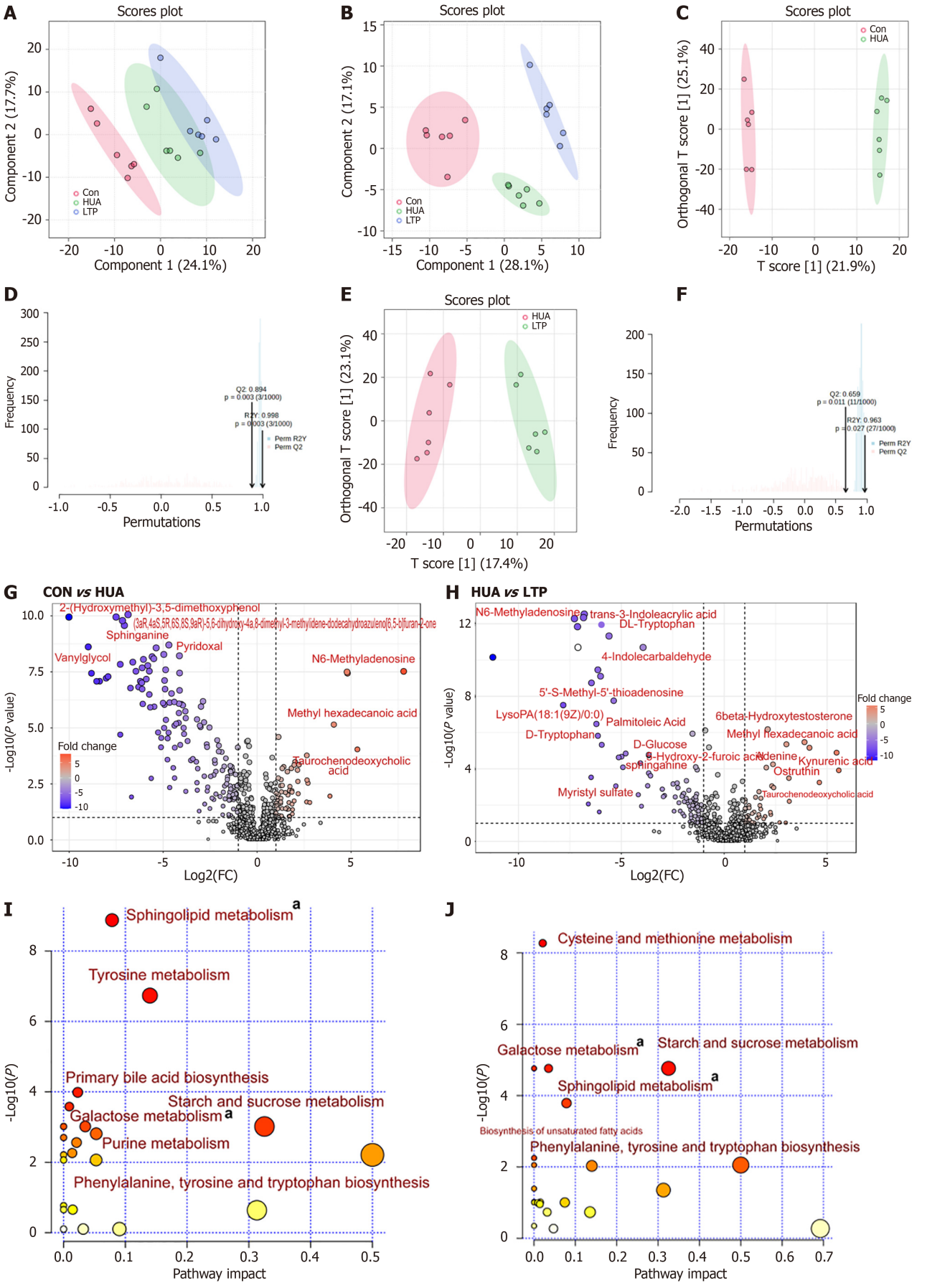

Figure 6 Leech *Poecilobdella manillensis* total protein extract alters the plasma metabolites in potassium oxonate-induced hyperuricemia mice. A and B: Partial least squares discriminant analysis (PLS-DA) score plots for normal control group (CON), hyperuricemia model group (HUA), and

leech *Poecilobdella manillensis* total protein extract treatment group (LTP) in positive and negative ion mode, respectively; C and D: Score plots and permutation tests of orthogonal PLS-DA (OPLS-DA) between the HUA and CON groups; E and F: Score plots and permutation tests of OPLS-DA between the LTP and HUA groups; G: Volcano plot showing most significant metabolites identified by univariate analysis between the HUA and CON groups; H: Volcano plot showing most significant metabolites identified by univariate analysis between the LTP and HUA groups; I: Summary plot for pathway analysis of CON *vs* HUA; J: Summary plot for pathway analysis of LTP *vs* HUA, a pathways coexisted in both the microbiota and metabolome. CON: Normal control group; HUA: Hyperuricemia model group; LTP: Leech *Poecilobdella manillensis* total protein extract treatment group; FC: Fold change.

lyophilized powder in the treatment of HUA in previous experiments, we extracted leech protein from leech *Poecilobdella manillensis* freeze-dried powder, and conducted an experiment focused on lowering UA through the administration of LTP to HUA mice. Consequently, the mechanism was expounded in relation to the gut microbiota and metabolites. We demonstrated the excellent curative potential of LTP with respect to lowering UA levels by decreasing urate synthesis and increasing renal urate excretion (summarized in Figure 10). To our knowledge, this is the first study to reveal that LTP could ameliorate the progression of HUA by re-programming the gut microbiome and metabolome.

LTP ameliorated disruptions in UA and renal function

Employing a yeast-based high-purine diet in conjunction with PO can emulate disturbances in purine metabolism, elevating UA levels and, thereby inducing an HUA model[34]. Our study employed PO alongside a yeast-based high-purine diet to successfully establish an HUA model in mice. Our findings provide evidence that LTP (as a lowering treatment for UA) induced beneficial physiological alterations in HUA-treated mice, manifesting as a noteworthy reduction in HUA-associated biochemical parameters (*e.g.*, serum UA, BUN, and CRE). Prior research has underscored the efficacy of hirudin in lowering serum UA and BUN levels and mitigating renal pathological damage[24]. Consistent with prior investigations, our study observed elevated serum CRE and BUN in the HUA mice; however, LTP treatment notably attenuated these levels, indicating that LTP ameliorated the disruptions in UA metabolism and mitigated the renal function impairment induced by HUA.

LTP enhanced UA excretion by decreasing urate synthesis and increasing renal urate excretion, thus ameliorating renal and intestinal barrier impairment

Our initial investigation into the impact of LTP on UA production unveiled its ability to attenuate XOD activity, consequently diminishing UA synthesis - a potential performance akin to AP. Our investigation highlighted that LTP not only reduced the renal concentrations of URAT1 and GLUT9 but also elevated kidney and jejunum ABCG2 proteins, in line with previous research[35]. This is related to the fact that renal UA clearance is mainly dependent on different transporters, including URAT1, GLUT9, and ABCG2[36]. Notably, the observation of the ABCG2 protein concentration in the jejunum in our study is consistent with previous reports showing that the ABCG2-encoded transporter BCRP plays a role in the gut[1]. In essence, our results delineate the dual action of LTP, *i.e.*, attenuating UA synthesis by inhibiting XOD activity and enhancing UA excretion by modulating distinct UA transporters in both the renal and intestinal domains.

Our investigation revealed decreases in ZO-1 and occludin levels in the renal tissue of HUA mice ($P < 0.05$). Following LTP treatment, a notable upward trend in the concentration of these proteins was observed ($P < 0.01$), signifying the ameliorative effect of LTP on renal barrier impairment in HUA mice. This aligns with previous findings suggesting that alterations in tight junctions play a crucial role during the repair of renal injury and participate in the pathophysiological processes involved in renal recovery[37]. The reason for this might be that aberrations in tight junctions lead to compromised integrity in the intestinal or renal epithelium, culminating in absorption and secretion disorders, consequently affecting UA excretion[38]. Likewise, our observations revealed a parallel correlation between ZO-1 and occludin within the jejunum tissue and the kidney tissue of the LTP group. However, the observed elevation of ZO-1 in the jejunum tissue of the AP group did not exhibit statistical significance. These outcomes suggest the concurrent impact of LTP on the tight junction proteins present in both the jejunum and kidney.

In this study, we particularly focused on the histological changes in liver and kidney tissues induced by the HUA model. The experimental results showed significant pathological changes in the renal interstitium of HUA mice, including swelling and atrophy of the renal tubules, irregular tubular lumens, and significant infiltration of monocytes and lymphocytes in the interstitium, which are clear signs of an inflammatory response. In contrast, the renal interstitial pathological structure of the LTP group showed a significant improvement. These observational findings confirm the potential efficacy of LTP in repairing renal barrier impairment caused by HUA.

Modulatory effects of LTP on the gut microbiota

The gut microbiome, which is often regarded as the 'second genome' acquired by the human body, constitutes a remarkably rich and functionally pivotal ecosystem, encompassing an estimated 10-100 trillion micro-organisms, including bacteria and viruses, residing within the human intestinal tract[39]. Disruptions in the structure of this intestinal flora could trigger metabolic dysregulation, which is intricately linked with HUA and gout[39]. The interplay between the intestinal flora and kidney diseases disrupts the equilibrium of gut microbes, leading to renal impairment [40]. In rat models of renal failure, a significant reduction in renal excretion triggers an adaptive discharge of UA into the intestinal lumen[41]. This process leads to marked changes in the composition and quantity of the gut microbiota[41]. In this study, our exploration of disease pathogenesis utilized the gut microbiota as a pivotal starting point. Given the intricate composition of intestinal micro-organisms, the impact of different microbial entities diverges significantly. Consequently, the efficacy of LTP in reducing UA levels cannot be solely attributed to the actions of a singular bacterium.

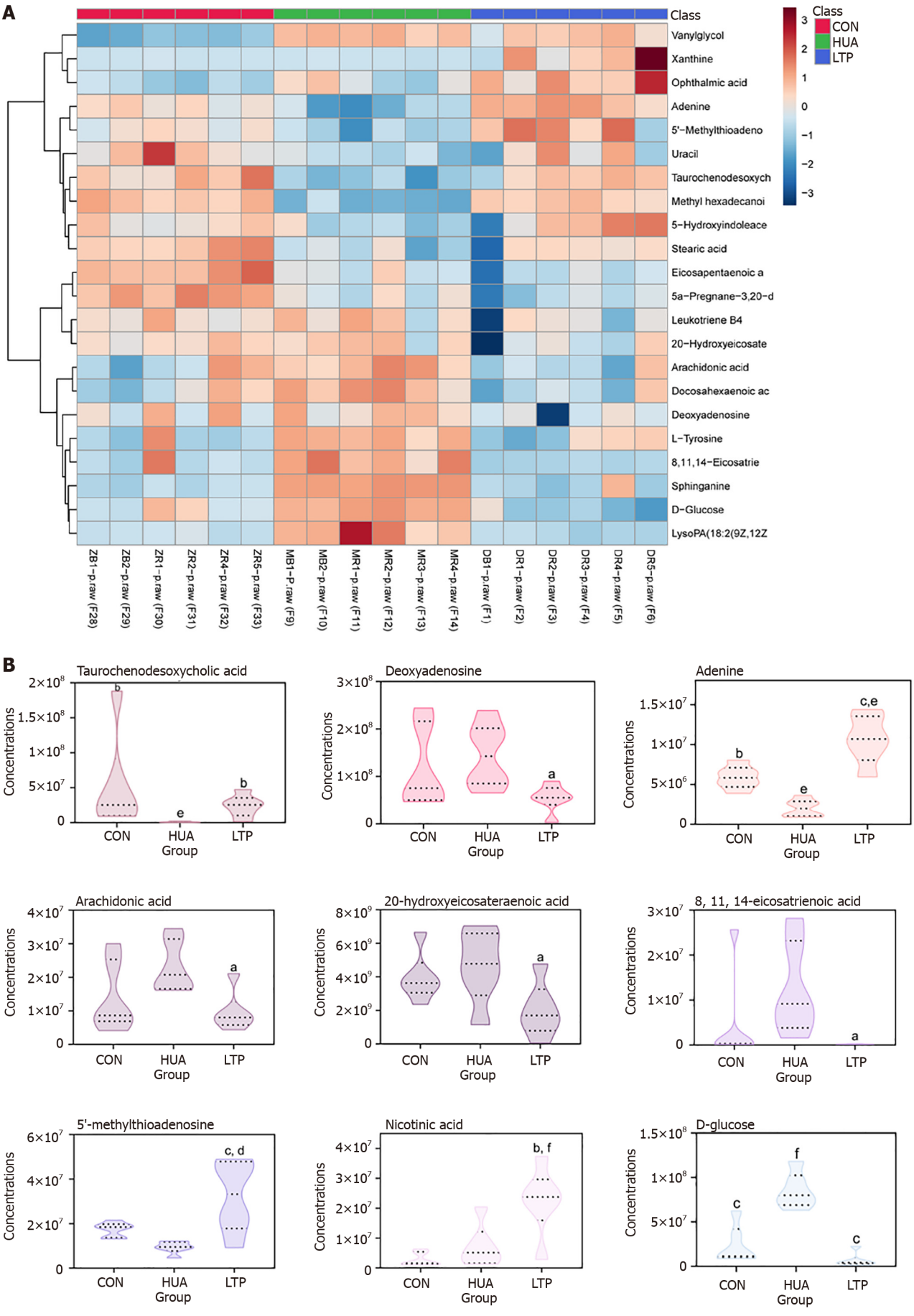
A
Class
CON
HUA
LTP
Vanylglycol
Xanthine
Ophthalmic acid
Adenine
5'-Methylthioadeno
Uracil
Taurochenodesoxych
Methyl hexadecanoi
5-Hydroxyindoleace
Stearic acid
Eicosapentaenoic a
5a-Pregnane-3,20-d
Leukotriene B4
20-Hydroxyeicosate
Arachidonic acid
Docosahexaenoic ac
Deoxyadenosine
L-Tyrosine
8,11,14-Eicosatrie
Sphinganine
D-Glucose
LysoPA(18:2(9Z,12Z
ZB1-p.raw (F28)
ZB2-p.raw (F29)
ZR1-p.raw (F30)
ZR2-p.raw (F31)
ZR4-p.raw (F32)
ZR5-p.raw (F33)
MB1-P.raw (F9)
MB2-p.raw (F10)
MR1-p.raw (F11)
MR2-p.raw (F12)
MR3-p.raw (F13)
MR4-p.raw (F14)
DB1-p.raw (F1)
DR1-p.raw (F2)
DR2-p.raw (F3)
DR3-p.raw (F4)
DR4-p.raw (F5)
DR5-p.raw (F6)
B
Taurochenodesoxycholic acid
Deoxyadenosine
Adenine
Arachidonic acid
20-hydroxyeicosateraenoic acid
8, 11, 14-eicosatrienoic acid
5'-methylthioadenosine
Nicotinic acid
D-glucose
Concentrations
CON
HUA
LTP
Group

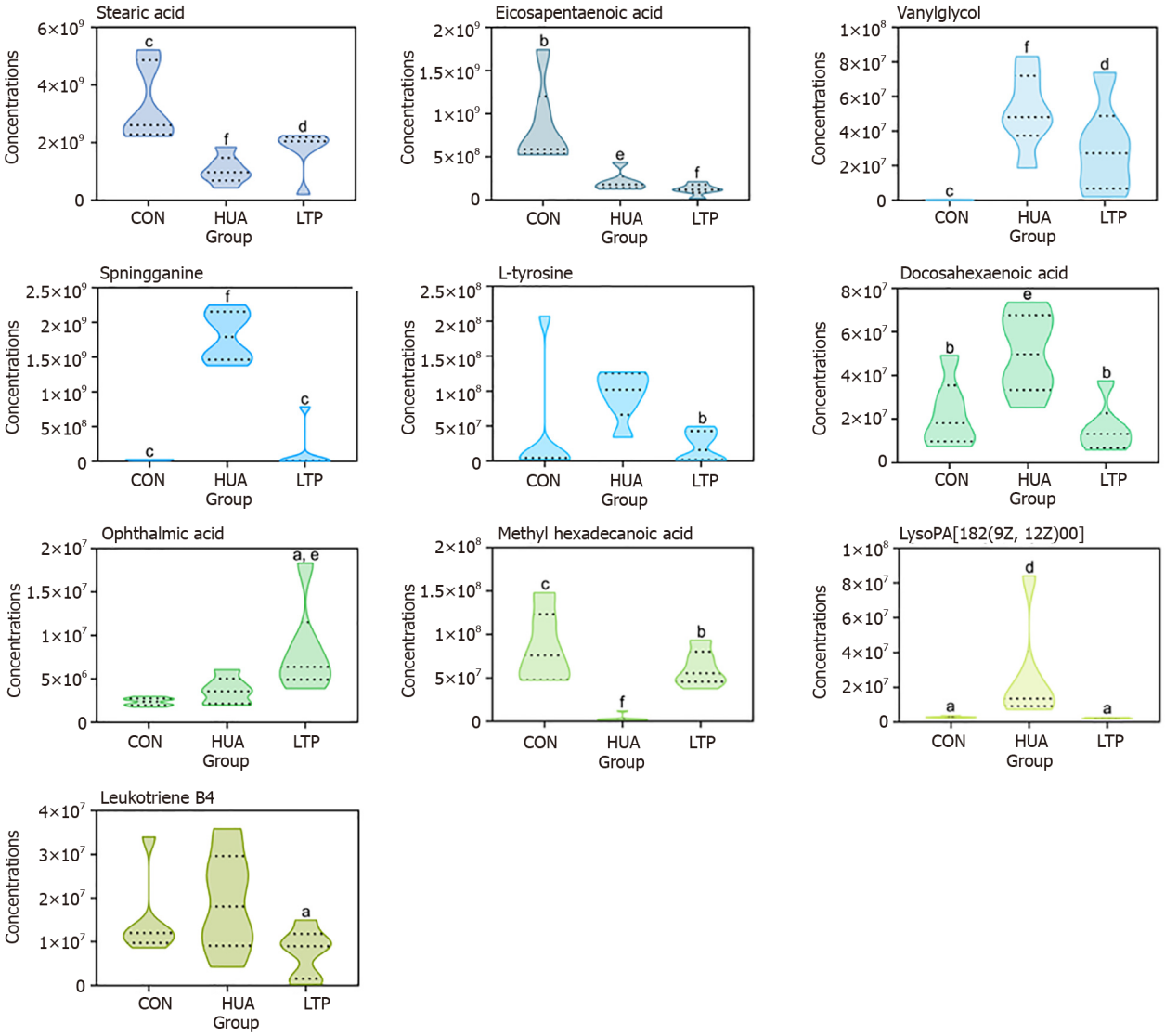

Figure 7 Effect of leech *Poecilobdella manillensis* total protein extract on vital metabolites. A: Heatmaps showing the trends in differential metabolites between groups; B: The concentrations of vital metabolites for all groups, assessed through the Kruskal-Wallis ANOVA. Statistical significance is indicated as follows: $^{a}P < 0.05$ *vs* hyperuricemia model group (HUA); $^{b}P < 0.01$ *vs* HUA; $^{c}P < 0.001$ *vs* HUA; $^{d}P < 0.05$ *vs* normal control group (CON); $^{e}P < 0.01$ *vs* CON; $^{f}P < 0.001$ *vs* CON. CON: Normal control group; HUA: Hyperuricemia model group; LTP: Leech *Poecilobdella manillensis* total protein extract treatment group.

Alterations in the microbiota structure have been observed in both human and animal models of HUA, notably at the phylum and genus levels[42,43]. The α- and β-diversity analyses of gut microbes conducted in this investigation showcased the capacity of LTP to enhance gut microbial diversity and influence the microbial structure in HUA mice. Specifically, at the phylum level, LTP administration led to a reduction in *Bacteroidota* and an elevation in the relative abundance of *Firmicutes*. This adjustment resulted in the restoration of the *Bacteroides* to *Firmicutes* ratio to a level akin to that in the CON group, thereby exerting a favorable influence on the restoration of the intestinal flora. These findings align with the conclusions drawn by Cao *et al*[44], emphasizing the pivotal role of the *Bacteroidetes* to *Firmicutes* ratio in preserving normal intestinal homeostasis and its association with HUA. It has been documented that *Faecalibacterium*, *Lactobacillus*, and *Bifidobacterium* represent pivotal core and physiological flora within the gastrointestinal tract of both humans and animals[45,46], which are capable of producing short-chain fatty acids, thereby fostering intestinal health through the reduction in oxidative stress, autophagic processes, and inflammation[45-47]. Additionally, *Clostridium_sensu_stricto_1* has demonstrated effective regulation of intestinal flora, being characterized as a dominant strain in cases of type 2 diabetes mellitus[48]. *Escherichia_Shigella* exhibited significant enrichment among long-lived healthy individuals[49]. Conversely, *Sphingomonas* species have been identified as opportunistic pathogens[50,51]. A study indicated that *Alloprevotella* is associated with inflammatory markers and represents a risk factor for sepsis[52]. In our study, a decline was observed in the relative abundance of *Lactobacillus*, *Faecalibacterium*, *Clostridium_sensu_stricto_1*, *Bifidobacterium*, and *Escherichia_Shigella* in HUA mice. Meanwhile, the relative abundance of *Alloprevotella* and *Sphingomonas* increased. Notably, the increase in *Alloprevotella* and *Sphingomonas*, alongside the observed changes in epithelial tight junction proteins, may suggest a potential weakening of the intestinal barrier, which could subsequently heighten the risk of intestinal inflammation and increase susceptibility to pathogenic invasion[53]. However, LTP treatment successfully reversed these shifts in the gut microbiota, notably augmenting the relative abundances of

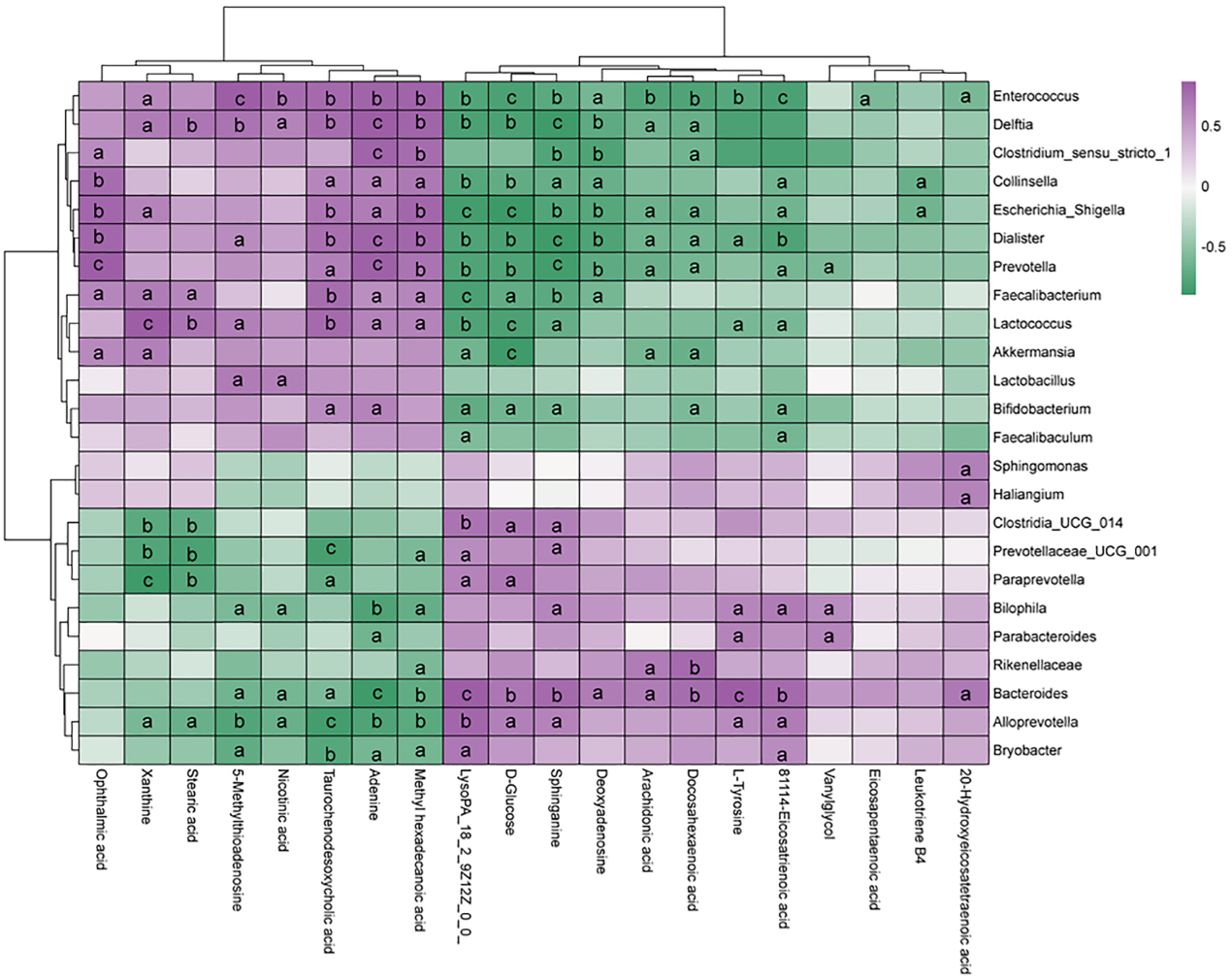

Figure 8 Correlation analysis between the gut microbiota and metabolites from hyperuricemia and leech *Poecilobdella manillensis* total protein extract groups. The R values are represented by gradient colors, where purple cells indicate positive correlations and green cells indicate negative correlations, respectively. Statistical significance is denoted as follows: $^{a}P < 0.05$, $^{b}P < 0.01$, $^{c}P < 0.001$.

beneficial probiotics such as *Lactobacillus*, *Faecalibacterium*, and *Bifidobacterium*. This indicates the potential role of LTP treatment in enhancing the integrity of the intestinal barrier by increasing the concentration of tight junction proteins, which may indirectly contribute to mitigating conditions associated with gut microbiota dysbiosis. *Prevotella*, a prominent member of the gut microbiome[54], exhibited a significantly lower abundance in HUA mice and a higher abundance in CON group mice. In particular, following LTP treatment, the relative abundance of *Prevotella* notably increased. This aligns with conclusions linking *Prevotellaceae UCG-001* to anti-inflammatory effects on immune cells and the inhibition of potential invasive pathogens[55]. *Dialister* was enriched following LTP treatment, consistent with clinical findings on beneficial bacteria related to depression[56]. *Akkermansia*, which was also notably enriched in the LTP group, belongs to a class of probiotics capable of enhancing the barrier function of the intestinal mucosa and reinforcing the host immune response[57]. In this study, the disruption of the balance of *Bacteroides* - which constituted a significant proportion in the genus - in HUA mice was evident when compared to the CON group. However, LTP intervention restored the relative abundance of *Bacteroides* to levels observed in the CON group, thus re-establishing the original balance of the gut microbiota. Spearman correlation analysis showed that *Enterococcus*, *Escherichia_Shigella*, *Delftia*, *Dialister*, *Prevotella*, and *Bacteroides* were strongly correlated with serum UA, serum CRE, liver XOD, URAT1, ABCG2, occludin, and ZO-1. In conclusion, LTP treatment not only fortified beneficial bacteria but also curtailed the relative abundance of harmful bacteria, restoring the equilibrium of intestinal microflora dominated by the largest bacterial proportion. These comprehensive analytical results highlight the dual role of LTP in the protection of both the renal and intestinal barriers, which is particularly important in addressing HUA and its complications. This finding provides an important theoretical basis for future clinical studies, especially when exploring LTP as a potential therapy for treating HUA and its related complications.

LTP demonstrated a modulatory impact on serum metabolites

Serum metabolomics analysis exhibited a notable amelioration in disturbed serum metabolism with LTP treatment. The screening process identified 22 metabolites linked with HUA, which were predominantly engaged in amino acid, lipid, and energy metabolism. Furthermore, these alterations were effectively reversed following LTP treatment in HUA mice.

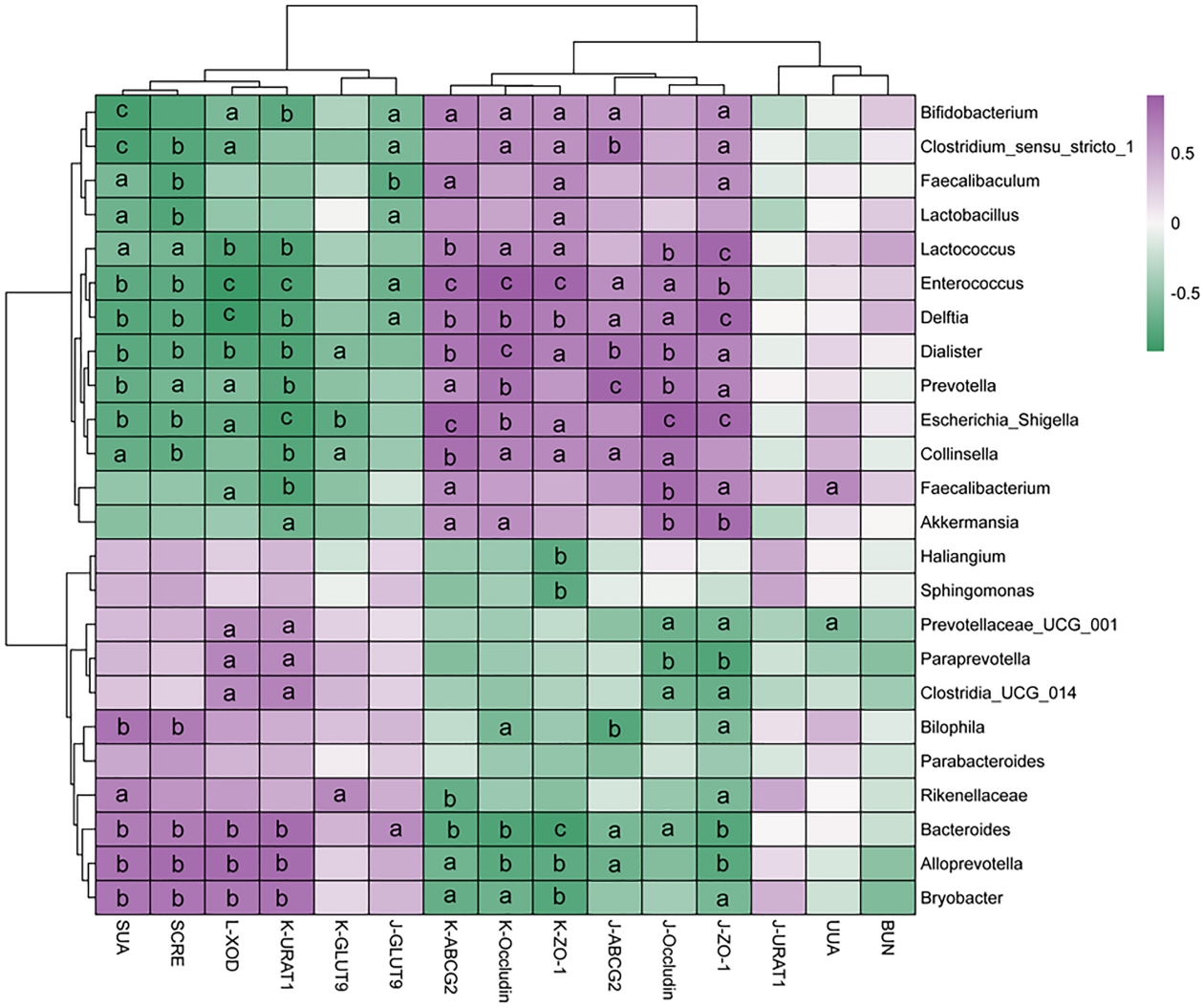

Figure 9 Correlation analysis between gut microbiota and hyperuricemia-related parameters. The R values are represented by gradient colors, where purple cells indicate positive correlations and green cells indicate negative correlations, respectively. Statistical significance is denoted as follows: $^{a}P < 0.05$, $^{b}P < 0.01$, $^{c}P < 0.001$. BUN: Blood urea nitrogen; UUA: Urinary uric acid; ZO-1: Zonula occludens-1; URAT1: Urate transporter 1; GLUT9: Glucose transporter 9; ABCG2: ATP-binding cassette transporter G2; XOD: Xanthine oxidase; SCRE: Serum creatinine; SUA: Serum uric acid.

These findings highlight the metabolic pathways intertwined with HUA and the capacity of LTP to enhance pertinent markers.

LTP reversal of HUA-induced lipid metabolic alterations: In this study, we focused on the alterations in sphinganine levels in the HUA model mouse. Sphinganine, a key intermediate metabolite in the sphingolipid metabolic pathway, showed a significant increase in the serum of HUA mice. This not only suggests a potential disruption in the regulatory functions of sphingolipid metabolism but also reflects a deeper biomarker of the metabolic disorder. Previous research has shown that metabolites from sphingolipids function as signaling molecules. These molecules regulate various processes associated with immune responses and inflammation[58]. Furthermore, there is evidence linking HUA with immune reactions and inflammatory processes[59]. Therefore, the sphingolipid metabolic pathway may contribute to the onset of HUA through its effects on immunity and inflammation, potentially due to elevated sphinganine levels increasing the synthesis of ceramide, a bioactive lipid signaling molecule known to significantly influence cellular signaling and inflammation control[60]. Recent studies have demonstrated that sphingolipids from intestinal bacteria can traverse the intestinal-epithelial barrier, thereby altering the sphingolipid metabolism of the host[61].

Our findings indicate that LTP treatment significantly ameliorated the increase in sphinganine, suggesting that modulation of the sphingolipid metabolic pathway by LTP could offer potential therapeutic effects on HUA. Specifically, LTP may decrease the production of sphinganine or enhance its clearance, thus influencing UA synthesis and excretion. Future research should further explore how LTP specifically affects sphinganine and related metabolites to deepen our understanding of its regulatory mechanisms on UA levels.

Furthermore, we observed significant negative correlations between specific microbial populations in the gut microbiota - such as *Delftia*, *Dialister*, *Clostridium_sensu_stricto_1*, *Escherichia_Shigella*, *Enterococcus*, and *Prevotella* - while *Bacteroides* showed a positive correlation. This suggests that the interaction between sphingolipid metabolism and gut microbiota may play a crucial role in the therapeutic effects of LTP on HUA, primarily through the modulation of gut

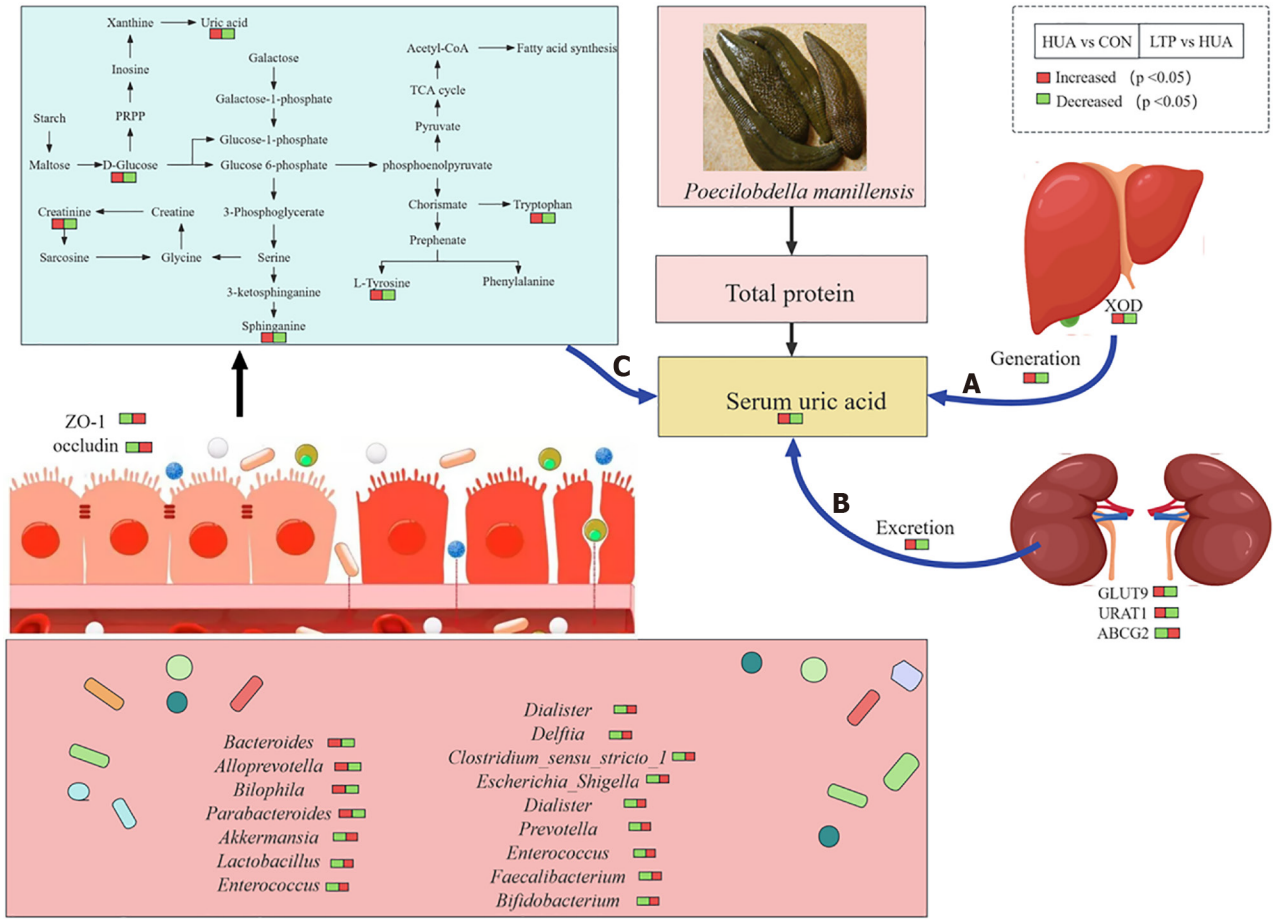

Figure 10 Mechanisms associated with treatment of *Poecilobdella manillensis* for hyperuricemia. A: decreased of uric acid generation in liver by reducing levels of xanthine oxidase; B: Reduction of uric acid excretion from kidney by regulating the expression of glucose transporter 9, urate transporter 1, and ATP-binding cassette transporter G2; C: Improvement of gut microbiota dysbiosis and regulation of sphingolipid metabolism and galactose metabolism. CON: Normal control group; HUA: Hyperuricemia model group; LTP: Leech *Poecilobdella manillensis* total protein extract treatment group; ZO-1: Zonula occludens-1; URAT1: Urate transporter 1; GLUT9: Glucose transporter 9; ABCG2: ATP-binding cassette transporter G2; XOD: Xanthine oxidase.

microbial communities affecting the sphingolipid metabolic pathway. These results not only provide new insights into the pathophysiological mechanisms of HUA but also offer a biological foundation for the development of novel therapeutic strategies based on the regulation of sphingolipid metabolism.

LTP reversed HUA-induced alterations in energy metabolism: LTP effectively reversed the disruptions in energy metabolism caused by high UA levels, as evidenced by our comprehensive functional enrichment analysis of the serum metabolome and gut microbiome. This analysis particularly highlighted the involvement of the galactose metabolism pathway, underscoring its pivotal role in mediating the therapeutic effects of LTP on HUA. LTP is suggested to exert its UA-lowering effects by modulating the gut microbiota, which, in turn, influences the galactose metabolic pathway intimately connected with glucose metabolism. This modulation may correct metabolic irregularities and restore metabolic equilibrium, offering a promising avenue for treating HUA.

In our study, elevated levels of D-glucose observed in HUA mice were significantly reduced following LTP treatment, suggesting LTP's potential role in regulating key metabolic pathways, such as the galactose metabolism pathway, alongside reducing UA levels. Although the direct link between galactose metabolism and UA levels has not been extensively documented in the literature, our findings may indicate a novel area of interest for further investigation into how specific metabolic pathways influence UA homeostasis. Notably, D-glucose - a critical metabolite within the galactose pathway - demonstrated significant correlations with various gut microbiota. It showed negative correlations with *Enterococcus*, *Escherichia_Shigella*, *Lactococcus*, *Delftia*, *Dialister*, *Prevotella*, and *Akkermansia*, and a positive correlation with *Bacteroides*.

These findings suggest that shifts in D-glucose levels may influence, or be influenced by, changes in the composition of the gut microbiota. LTP selectively enhances the abundance of these microbiota, potentially through the modulation of the galactose metabolic pathway, which is linked to glucose metabolism. This highlights a complex interplay between metabolic pathways and microbiota that may be key to developing new treatments for metabolic diseases.

CONCLUSION

In conclusion, based on the results of multiple omics studies, LTP was found to play a therapeutic role in HUA by regulating gut microbial homeostasis and serum metabolites. We found that LTP might influence the gut microbiota to act on sphingolipid metabolism and galactose metabolism pathways, facilitating UA-lowering therapy. Our findings are expected to promote further research on the regulatory effects of LTP on the gut microbiome and serum metabolomics, providing new insights into microbiome-based HUA treatment strategies.

FOOTNOTES

Author contributions: Liu X, Liang XQ, Lu TC, and Wang LS designed the research study; Liu X, Liang XQ, and Wang LS performed the research and wrote the original draft; Feng Z, Zhang M, and Wang B conducted the investigations; Liu X, Zhang FL, Wang B, and Wang LS developed the methodologies; Zhang M, Liao NQ, Zhang FL, and Wang LS managed the software used; Lu TC and Wang LS acquired the funding; Lu TC, Feng Z, and Wang LS administered the project and supervised the project; Liu X, Zhang FL, and Wang B validated the results; Liu X and Wang LS reviewed and edited the manuscript. All authors have read and approved the final manuscript.

Supported by National Natural Science Foundation of China, No. 82160843.

Institutional animal care and use committee statement: All procedures involving animals were reviewed and approved by the Attitude of Animal Care & Welfare Committee of Guangxi University (No. GXU-2023-0203).

Conflict-of-interest statement: All the authors report no relevant conflicts of interest for this article.

Data sharing statement: Technical appendix, statistical code, and dataset available from the corresponding author at lswang@gxu.edu.cn.

ARRIVE guidelines statement: The authors have read the ARRIVE guidelines, and the manuscript was prepared and revised according to the ARRIVE guidelines.

Country of origin: China

ORCID number: Xia Liu 0009-0007-8237-248X; Xing-Qiu Liang 0000-0003-3378-1336; Zhe Feng 0009-0005-7032-0012; Li-Sheng Wang 0000-0003-2655-0724.

S-Editor: Wang JJ
L-Editor: A
P-Editor: Yu HG

REFERENCES

1 **Zhao H**, Chen X, Zhang L, Meng F, Zhou L, Pang X, Lu Z, Lu Y. Lacticaseibacillus rhamnosus Fmb14 prevents purine induced hyperuricemia and alleviate renal fibrosis through gut-kidney axis. *Pharmacol Res* 2022; **182**: 106350 [PMID: 35843568 DOI: 10.1016/j.phrs.2022.106350]
2 **Li S**, Liu X, Jia X, Fang M, Yang Q, Gong Z. Assessment of the temporal trend and daily profiles of the dietary purine intake among Chinese residents during 2014 to 2021. *Front Nutr* 2023; **10**: 1259053 [PMID: 38024389 DOI: 10.3389/fnut.2023.1259053]
3 **Yanai H**, Adachi H, Hakoshima M, Katsuyama H. Molecular Biological and Clinical Understanding of the Pathophysiology and Treatments of Hyperuricemia and Its Association with Metabolic Syndrome, Cardiovascular Diseases and Chronic Kidney Disease. *Int J Mol Sci* 2021; **22** [PMID: 34502127 DOI: 10.3390/ijms22179221]
4 **McCormick N**, Lin K, Yokose C, Lu N, Zhang Y, Choi HK. Unclosing Premature Mortality Gap Among Patients With Gout in the US General Population, Independent of Serum Urate and Atherosclerotic Cardiovascular Risk Factors. *Arthritis Care Res (Hoboken)* 2024; **76**: 691-702 [PMID: 38191784 DOI: 10.1002/acr.25292]
5 **Agus A**, Clément K, Sokol H. Gut microbiota-derived metabolites as central regulators in metabolic disorders. *Gut* 2021; **70**: 1174-1182 [PMID: 33272977 DOI: 10.1136/gutjnl-2020-323071]
6 **Wang Z**, Li Y, Liao W, Huang J, Liu Y, Li Z, Tang J. Gut microbiota remodeling: A promising therapeutic strategy to confront hyperuricemia and gout. *Front Cell Infect Microbiol* 2022; **12**: 935723 [PMID: 36034697 DOI: 10.3389/fcimb.2022.935723]
7 **Sun X**, Wen J, Guan B, Li J, Luo J, Li J, Wei M, Qiu H. Folic acid and zinc improve hyperuricemia by altering the gut microbiota of rats with high-purine diet-induced hyperuricemia. *Front Microbiol* 2022; **13**: 907952 [PMID: 35966674 DOI: 10.3389/fmicb.2022.907952]
8 **Wang K**, Zhang Z, Hang J, Liu J, Guo F, Ding Y, Li M, Nie Q, Lin J, Zhuo Y, Sun L, Luo X, Zhong Q, Ye C, Yun C, Zhang Y, Wang J, Bao R, Pang Y, Wang G, Gonzalez FJ, Lei X, Qiao J, Jiang C. Microbial-host-isozyme analyses reveal microbial DPP4 as a potential antidiabetic target. *Science* 2023; **381**: eadd5787 [PMID: 37535747 DOI: 10.1126/science.add5787]
9 **Chen Y**, Pei C, Chen Y, Xiao X, Zhang X, Cai K, Deng S, Liang R, Xie Z, Li P, Liao Q. Kidney tea ameliorates hyperuricemia in mice *via* altering gut microbiota and restoring metabolic profile. *Chem Biol Interact* 2023; **376**: 110449 [PMID: 36921834 DOI:

10.1016/j.cbi.2023.110449]
10 **Wang J**, Chen Y, Zhong H, Chen F, Regenstein J, Hu X, Cai L, Feng F. The gut microbiota as a target to control hyperuricemia pathogenesis: Potential mechanisms and therapeutic strategies. *Crit Rev Food Sci Nutr* 2022; **62**: 3979-3989 [PMID: 33480266 DOI: 10.1080/10408398.2021.1874287]
11 **Song S**, Lou Y, Mao Y, Wen X, Fan M, He Z, Shen Y, Wen C, Shao T. Alteration of Gut Microbiome and Correlated Amino Acid Metabolism Contribute to Hyperuricemia and Th17-Driven Inflammation in Uox-KO Mice. *Front Immunol* 2022; **13**: 804306 [PMID: 35197978 DOI: 10.3389/fimmu.2022.804306]
12 **Sapankaew T**, Thadanipon K, Ruenroengbun N, Chaiyakittisopon K, Ingsathit A, Numthavaj P, Chaiyakunapruk N, McKay G, Attia J, Thakkinstian A. Efficacy and safety of urate-lowering agents in asymptomatic hyperuricemia: systematic review and network meta-analysis of randomized controlled trials. *BMC Nephrol* 2022; **23**: 223 [PMID: 35739495 DOI: 10.1186/s12882-022-02850-3]
13 **Strilchuk L**, Fogacci F, Cicero AF. Safety and tolerability of available urate-lowering drugs: a critical review. *Expert Opin Drug Saf* 2019; **18**: 261-271 [PMID: 30915866 DOI: 10.1080/14740338.2019.1594771]
14 **Anis TR**, Meher J. Allopurinol-Induced Stevens-Johnson Syndrome (SJS). *Clin Pharmacol* 2023; **15**: 99-105 [PMID: 37811521 DOI: 10.2147/CPAA.S427714]
15 **Viel S**, Pescarmona R, Belot A, Nosbaum A, Lombard C, Walzer T, Bérard F. A Case of Type 2 Hypersensitivity to Rasburicase Diagnosed with a Natural Killer Cell Activation Assay. *Front Immunol* 2018; **9**: 110 [PMID: 29434608 DOI: 10.3389/fimmu.2018.00110]
16 **Cheuk DK**, Chiang AK, Chan GC, Ha SY. Urate oxidase for the prevention and treatment of tumour lysis syndrome in children with cancer. *Cochrane Database Syst Rev* 2017; **3**: CD006945 [PMID: 28272834 DOI: 10.1002/14651858.CD006945.pub4]
17 **Fan JX**, Liu JY, Gao Y, Liu SQ. [Research on the mechanism of leech preparation in the treatment of stroke]. *Yaoxve Yanjiu* 2023 [DOI: 10.13506/j.cnki.jpr.2023.01.009]
18 **Wang C**, Chen M, Lu X, Yang S, Yang M, Fang Y, Lai R, Duan Z. Isolation and Characterization of Poeciguamerin, a Peptide with Dual Analgesic and Anti-Thrombotic Activity from the Poecilobdella manillensis Leech. *Int J Mol Sci* 2023; **24** [PMID: 37446275 DOI: 10.3390/ijms241311097]
19 **Qiu J**, Lingna W, Jinghong H, Yongqing Z. Oral administration of leeches (Shuizhi): A review of the mechanisms of action on antiplatelet aggregation. *J Ethnopharmacol* 2019; **232**: 103-109 [PMID: 30543914 DOI: 10.1016/j.jep.2018.12.010]
20 **Sig AK**, Guney M, Uskudar Guclu A, Ozmen E. Medicinal leech therapy-an overall perspective. *Integr Med Res* 2017; **6**: 337-343 [PMID: 29296560 DOI: 10.1016/j.imr.2017.08.001]
21 **Rodriguez-Merchan EC**. Topical therapies for knee osteoarthritis. *Postgrad Med* 2018; **130**: 607-612 [PMID: 30156934 DOI: 10.1080/00325481.2018.1505182]
22 **Dong YY**, Liu YK, Deng XL, Liang J. [Mechanism of Poecilobdella Manillensis Lyophilized Powder on Hyperuricemia Based on Network Pharmacology, RNA-seq Technology and Experimental Validation]. *Zhongguo Xiandai Yingyun Yaoxve* 2024 [DOI: 10.13748/j.cnki.issn1007-7693.20230100]
23 **Grafskaia EN**, Pavlova ER, Latsis IA, Malakhova MV, Ivchenkov DV, Bashkirov PV, Kot EF, Mineev KS, Arseniev AS, Klinov DV, Lazarev VN. Non-toxic antimicrobial peptide Hm-AMP2 from leech metagenome proteins identified by the gradient-boosting approach. *Mater Des* 2022; **224**: 111364 [DOI: 10.1016/j.matdes.2022.111364]
24 **Junren C**, Xiaofang X, Huiqiong Z, Gangmin L, Yanpeng Y, Xiaoyu C, Yuqing G, Yanan L, Yue Z, Fu P, Cheng P. Pharmacological Activities and Mechanisms of Hirudin and Its Derivatives - A Review. *Front Pharmacol* 2021; **12**: 660757 [PMID: 33935784 DOI: 10.3389/fphar.2021.660757]
25 **Sun Y**, Wang B, Pei J, Luo Y, Yuan N, Xiao Z, Wu H, Luo C, Wang J, Wei S, Pei Y, Fu S, Wang D. Molecular dynamic and pharmacological studies on protein-engineered hirudin variants of Hirudinaria manillensis and Hirudo medicinalis. *Br J Pharmacol* 2022; **179**: 3740-3753 [PMID: 35135035 DOI: 10.1111/bph.15816]
26 **Wang YP**. [Isolation and Production of Antler Plate Protein from Sika Deer and preliminary study on its Bacteriostatic Mechanism of E.coil]. Jilin Agricultural University 2021
27 **Wang YT**. Study on the Purification and Characterization of Fibrinolytic Active Protein of American Cockroach. 2020
28 Wang YP, Zhou YJ, Hu W. [Isolation and purification of antler plate protein from Sika deer and preliminary study on its bacteriostatic mechanism against Escherichia coli]. *Shanghai Zhongyiyao Zazhi* 2021; **55**
29 **Liu J**, Gao M, He J, Wu K, Lin S, Jin L, Chen Y, Liu H, Shi J, Wang X, Chang L, Lin Y, Zhao YL, Zhang X, Zhang M, Luo GZ, Wu G, Pei D, Wang J, Bao X, Chen J. The RNA m(6)A reader YTHDC1 silences retrotransposons and guards ES cell identity. *Nature* 2021; **591**: 322-326 [PMID: 33658714 DOI: 10.1038/s41586-021-03313-9]
30 **Wang J**, Zhao J, Yan C, Xi C, Wu C, Zhao J, Li F, Ding Y, Zhang R, Qi S, Li X, Liu C, Hou W, Chen H, Wang Y, Wu D, Chen K, Jiang H, Huang H, Liu H. Identification and evaluation of a lipid-lowering small compound in preclinical models and in a Phase I trial. *Cell Metab* 2022; **34**: 667-680.e6 [PMID: 35427476 DOI: 10.1016/j.cmet.2022.03.006]
31 **Li K**, Lin C, Li M, Xu K, He Y, Mao Y, Lu L, Geng W, Li X, Luo Z, Cai K. Multienzyme-like Reactivity Cooperatively Impairs Glutathione Peroxidase 4 and Ferroptosis Suppressor Protein 1 Pathways in Triple-Negative Breast Cancer for Sensitized Ferroptosis Therapy. *ACS Nano* 2022; **16**: 2381-2398 [PMID: 35041395 DOI: 10.1021/acsnano.1c08664]
32 **Zou Y**, Sun X, Yang Q, Zheng M, Shimoni O, Ruan W, Wang Y, Zhang D, Yin J, Huang X, Tao W, Park JB, Liang XJ, Leong KW, Shi B. Blood-brain barrier-penetrating single CRISPR-Cas9 nanocapsules for effective and safe glioblastoma gene therapy. *Sci Adv* 2022; **8**: eabm8011 [PMID: 35442747 DOI: 10.1126/sciadv.abm8011]
33 **Wang H**, Zhao X, Tan L, Zhu J, Hyten D. Crop DNA extraction with lab-made magnetic nanoparticles. *PLoS One* 2024; **19**: e0296847 [PMID: 38190402 DOI: 10.1371/journal.pone.0296847]
34 **Sun L**, Liu Q, Zhang Y, Xue M, Yan H, Qiu X, Tian Y, Zhang H, Liang H. Fucoidan from Saccharina japonica Alleviates Hyperuricemia-Induced Renal Fibrosis through Inhibiting the JAK2/STAT3 Signaling Pathway. *J Agric Food Chem* 2023; **71**: 11454-11465 [PMID: 37481747 DOI: 10.1021/acs.jafc.3c01349]
35 **Han J**, Zuo Z, Shi X, Zhang Y, Peng Z, Xing Y, Pang X. Hirudin ameliorates diabetic nephropathy by inhibiting Gsdmd-mediated pyroptosis. *Cell Biol Toxicol* 2023; **39**: 573-589 [PMID: 34212273 DOI: 10.1007/s10565-021-09622-z]
36 **Banerjee M**, Mukhopadhyay S. Gout. *N Engl J Med* 2023; **388**: e47 [PMID: 36988610 DOI: 10.1056/NEJMc2216467]
37 **Xu X**, Zhang X, Gao L, Liu C, You K. Neonatal Hyperoxia Downregulates Claudin-4, Occludin, and ZO-1 Expression in Rat Kidney Accompanied by Impaired Proximal Tubular Development. *Oxid Med Cell Longev* 2020; **2020**: 2641461 [PMID: 33343804 DOI: 10.1155/2020/2641461]

38 **Sun H**, Li H, Yan J, Wang X, Xu M, Wang M, Fan B, Liu J, Lin N, Wang X, Li L, Zhao S, Gong Y. Loss of CLDN5 in podocytes deregulates WIF1 to activate WNT signaling and contributes to kidney disease. *Nat Commun* 2022; **13**: 1600 [PMID: 35332151 DOI: 10.1038/s41467-022-29277-6]

39 **Zhu C**, Niu H, Bian M, Zhang X, Zhang X, Zhou Z. Study on the mechanism of Orthosiphon aristatus (Blume) Miq. in the treatment of hyperuricemia by microbiome combined with metabonomics. *J Ethnopharmacol* 2023; **317**: 116805 [PMID: 37355082 DOI: 10.1016/j.jep.2023.116805]

40 **Ma Y**, Liu X, Wang J. Small molecules in the big picture of gut microbiome-host cross-talk. *EBioMedicine* 2022; **81**: 104085 [PMID: 35636316 DOI: 10.1016/j.ebiom.2022.104085]

41 **Altamura S**, Pietropaoli D, Lombardi F, Del Pinto R, Ferri C. An Overview of Chronic Kidney Disease Pathophysiology: The Impact of Gut Dysbiosis and Oral Disease. *Biomedicines* 2023; **11** [PMID: 38002033 DOI: 10.3390/biomedicines11113033]

42 **Halimulati M**, Wang R, Aihemaitijiang S, Huang X, Ye C, Zhang Z, Li L, Zhu W, Zhang Z, He L. Anti-Hyperuricemic Effect of Anserine Based on the Gut-Kidney Axis: Integrated Analysis of Metagenomics and Metabolomics. *Nutrients* 2023; **15** [PMID: 36839325 DOI: 10.3390/nu15040969]

43 **Yuan X**, Chen R, Zhang Y, Lin X, Yang X. Altered Gut Microbiota in Children With Hyperuricemia. *Front Endocrinol (Lausanne)* 2022; **13**: 848715 [PMID: 35574004 DOI: 10.3389/fendo.2022.848715]

44 **Cao J**, Liu Q, Hao H, Bu Y, Tian X, Wang T, Yi H. Lactobacillus paracasei X11 Ameliorates Hyperuricemia and Modulates Gut Microbiota in Mice. *Front Immunol* 2022; **13**: 940228 [PMID: 35874662 DOI: 10.3389/fimmu.2022.940228]

45 **Mao G**, Li S, Orfila C, Shen X, Zhou S, Linhardt RJ, Ye X, Chen S. Depolymerized RG-I-enriched pectin from citrus segment membranes modulates gut microbiota, increases SCFA production, and promotes the growth of Bifidobacterium spp., Lactobacillus spp. and Faecalibaculum spp. *Food Funct* 2019; **10**: 7828-7843 [PMID: 31778135 DOI: 10.1039/c9fo01534e]

46 **Martín R**, Rios-Covian D, Huillet E, Auger S, Khazaal S, Bermúdez-Humarán LG, Sokol H, Chatel JM, Langella P. Faecalibacterium: a bacterial genus with promising human health applications. *FEMS Microbiol Rev* 2023; **47** [PMID: 37451743 DOI: 10.1093/femsre/fuad039]

47 **Yi X**, Cai R, Shaoyong W, Wang G, Yan W, He Z, Li R, Chao M, Zhao T, Deng L, Yang G, Pang W. Melatonin promotes gut anti-oxidative status in perinatal rat by remodeling the gut microbiome. *Redox Biol* 2023; **65**: 102829 [PMID: 37527604 DOI: 10.1016/j.redox.2023.102829]

48 **Que Y**, Cao M, He J, Zhang Q, Chen Q, Yan C, Lin A, Yang L, Wu Z, Zhu D, Chen F, Chen Z, Xiao C, Hou K, Zhang B. Gut Bacterial Characteristics of Patients With Type 2 Diabetes Mellitus and the Application Potential. *Front Immunol* 2021; **12**: 722206 [PMID: 34484230 DOI: 10.3389/fimmu.2021.722206]

49 **Pang S**, Chen X, Lu Z, Meng L, Huang Y, Yu X, Huang L, Ye P, Chen X, Liang J, Peng T, Luo W, Wang S. Longevity of centenarians is reflected by the gut microbiome with youth-associated signatures. *Nat Aging* 2023; **3**: 436-449 [PMID: 37117794 DOI: 10.1038/s43587-023-00389-y]

50 **Johnson RC**, Deming C, Conlan S, Zellmer CJ, Michelin AV, Lee-Lin S, Thomas PJ, Park M, Weingarten RA, Less J, Dekker JP, Frank KM, Musser KA, McQuiston JR, Henderson DK, Lau AF, Palmore TN, Segre JA. Investigation of a Cluster of Sphingomonas koreensis Infections. *N Engl J Med* 2018; **379**: 2529-2539 [PMID: 30586509 DOI: 10.1056/NEJMoa1803238]

51 **Ryan MP**, Adley CC. Sphingomonas paucimobilis: a persistent Gram-negative nosocomial infectious organism. *J Hosp Infect* 2010; **75**: 153-157 [PMID: 20434794 DOI: 10.1016/j.jhin.2010.03.007]

52 **Chen JH**, Zeng LY, Zhao YF, Tang HX, Lei H, Wan YF, Deng YQ, Liu KX. Causal effects of gut microbiota on sepsis: a two-sample Mendelian randomization study. *Front Microbiol* 2023; **14**: 1167416 [PMID: 37234519 DOI: 10.3389/fmicb.2023.1167416]

53 **Yin L**, Huang G, Khan I, Su L, Xia W, Law BYK, Wong VKW, Wu Q, Wang J, Leong WK, Hsiao WLW. Poria cocos polysaccharides exert prebiotic function to attenuate the adverse effects and improve the therapeutic outcome of 5-FU in Apc(Min/+) mice. *Chin Med* 2022; **17**: 116 [PMID: 36192796 DOI: 10.1186/s13020-022-00667-8]

54 **Tett A**, Pasolli E, Masetti G, Ercolini D, Segata N. Prevotella diversity, niches and interactions with the human host. *Nat Rev Microbiol* 2021; **19**: 585-599 [PMID: 34050328 DOI: 10.1038/s41579-021-00559-y]

55 **Zhou X**, Zhang B, Zhao X, Lin Y, Wang J, Wang X, Hu N, Wang S. Chlorogenic acid supplementation ameliorates hyperuricemia, relieves renal inflammation, and modulates intestinal homeostasis. *Food Funct* 2021; **12**: 5637-5649 [PMID: 34018499 DOI: 10.1039/d0fo03199b]

56 **Chi L**, Khan I, Lin Z, Zhang J, Lee MYS, Leong W, Hsiao WLW, Zheng Y. Fructo-oligosaccharides from Morinda officinalis remodeled gut microbiota and alleviated depression features in a stress rat model. *Phytomedicine* 2020; **67**: 153157 [PMID: 31896054 DOI: 10.1016/j.phymed.2019.153157]

57 **Zhai Q**, Feng S, Arjan N, Chen W. A next generation probiotic, Akkermansia muciniphila. *Crit Rev Food Sci Nutr* 2019; **59**: 3227-3236 [PMID: 30373382 DOI: 10.1080/10408398.2018.1517725]

58 **Maceyka M**, Spiegel S. Sphingolipid metabolites in inflammatory disease. *Nature* 2014; **510**: 58-67 [PMID: 24899305 DOI: 10.1038/nature13475]

59 **Li D**, Yuan S, Deng Y, Wang X, Wu S, Chen X, Li Y, Ouyang J, Lin D, Quan H, Fu X, Li C, Mao W. The dysregulation of immune cells induced by uric acid: mechanisms of inflammation associated with hyperuricemia and its complications. *Front Immunol* 2023; **14**: 1282890 [PMID: 38053999 DOI: 10.3389/fimmu.2023.1282890]

60 **Jin J**, Lu Z, Li Y, Ru JH, Lopes-Virella MF, Huang Y. LPS and palmitate synergistically stimulate sphingosine kinase 1 and increase sphingosine 1 phosphate in RAW264.7 macrophages. *J Leukoc Biol* 2018; **104**: 843-853 [PMID: 29882996 DOI: 10.1002/JLB.3A0517-188RRR]

61 **Johnson EL**, Heaver SL, Waters JL, Kim BI, Bretin A, Goodman AL, Gewirtz AT, Worgall TS, Ley RE. Sphingolipids produced by gut bacteria enter host metabolic pathways impacting ceramide levels. *Nat Commun* 2020; **11**: 2471 [PMID: 32424203 DOI: 10.1038/s41467-020-16274-w]

Published by **Baishideng Publishing Group Inc**
7041 Koll Center Parkway, Suite 160, Pleasanton, CA 94566, USA
Telephone: +1-925-3991568
E-mail: office@baishideng.com
Help Desk: https://www.f6publishing.com/helpdesk
https://www.wjgnet.com